Full length article

Injectable nanofiber microspheres modified with metal phenolic networks for effective osteoarthritis treatment

Yujie Chen [a,1], Wei Xu [b,c,d,1], Muhammad Shafiq [a,e,*], Daiying Song [b,c], Tao Wang [f], Zhengchao Yuan [a], Xianrui Xie [g], Xiao Yu [a], Yihong Shen [a], Binbin Sun [a], Yu Liu [b,c,*], Xiumei Mo [a,*]

[a] Shanghai Engineering Research Center of Nano-Biomaterials and Regenerative Medicine, State Key Laboratory for Modification of Chemical Fibers and Polymer Materials, College of Biological Science and Medical Engineering, Donghua University, Songjiang, Shanghai 201600, China
[b] Research Institute of Plastic Surgery, Wei Fang Medical College, Weifang 261000, China
[c] Shanghai Key Laboratory of Tissue Engineering, Department of Plastic and Reconstructive Surgery, Shanghai 9th People's Hospital, Shanghai Stem Cell Institute, Shanghai Jiao Tong University School of Medicine, Huangpu, Shanghai 200001, China
[d] Department of Plastic Surgery, Qilu Hospital (Qingdao), Cheeloo College of Medicine, Shandong University, 758 Hefei Road, Qingdao, Shandong 266035, China
[e] Department of Chemical Engineering, Faculty of Engineering, Graduate School, Kyushu University, 744 Motooka, Nishi-ku, Fukuoka 819-0395, Japan
[f] Department of Plastic and Cosmetic Surgery, Shanghai Tongji Hospital, Tongji University School of Medicine, Shanghai 200001, China
[g] School of Pharmacy, Key Laboratory of Prescription Effect and Clinical Evaluation of State Administration of Traditional Chinese Medicine of China, Binzhou Medical University, Yantai 264003, China

ARTICLE INFO

ABSTRACT

Osteoarthritis (OA) is one of the most common chronic musculoskeletal diseases, which accounts for a large proportion of physical disabilities worldwide. Herein, we fabricated injectable gelatin/poly(L-lactide)-based nanofibrous microspheres (MS) via electrospraying technology, which were further modified with tannic acid (TA) named as TMS or metal phenolic networks (MPNs) consisting of TA and strontium ions (Sr^{2+}) and named as TSMS to enhance their bioactivity for OA therapy. The TA-modified microspheres exhibited stable porous structure and anti-oxidative activity. Notably, TSMS showed a sustained release of TA as compared to TMS, which exhibited a burst release of TA. While all types of microspheres exhibited good cytocompatibility, TSMS displayed good anti-inflammatory properties with higher cell viability and cartilage-related extracellular matrix (ECM) secretion. The TSMS microspheres also showed less apoptosis of chondrocytes in the hydrogen peroxide (H_2O_2)-induced inflammatory environment. The TSMS also inhibited the degradation of cartilage along with the considerable repair outcome in the papain-induced OA rabbit model in vivo as well as suppressed the expression level of inflammatory cytokines, such as tumor necrosis factor-alpha (TNF-α) and interleukin-1-beta (IL-1β). Taken together, TSMS may provide a highly desirable therapeutic option for intra-articular treatment of OA.

Statement of significance

Osteoarthritis (OA) is a chronic disease, which is caused by the inflammation of joint. Current treatments for OA achieve pain relief but hardly prevent or slow down the disease progression. Microspheres are at the forefront of drug delivery and tissue engineering applications, which can also be minimal-invasively injected into the joint. Polyphenols and therapeutic ions have been shown to be beneficial for the treatment of diseases related to the joints, including OA. Herein, we prepared gelatin/poly(L-lactide)-based nanofibrous microspheres (MS) via electrospinning incorporated electrospraying technology and functionalized them with the metal phenolic networks (MPNs) consisting of TA and strontium ions (Sr^{2+}), and assessed their potential for OA therapy both in vitro and in vivo.

---

* Corresponding authors.
  E-mail addresses: shafiqdr786@yahoo.com (M. Shafiq), yuliu1211@163.com (Y. Liu), xmm@dhu.edu.cn (X. Mo).

[1] These authors contributed equally to this work.

1. Introduction

Osteoarthritis (OA), a chronic disease caused by the inflammation of joints, poses severe health concerns as well as discomfort worldwide [1,2]. While not being fatal, the inflammatory mediators produced by the OA may induce the degeneration of different types of tissues and organs of the musculoskeletal system, such as synovium, bone, and cartilage if not appropriately intervened [3]. Current therapeutic treatments of OA involve surgical intervention, symptom control, delivery of oral analgesics and anti-inflammatory drugs, as well as non-pharmacological treatments (e.g. self-management, advice to lose weight, etc.) [4]. While these therapeutic modalities achieve pain relief, most of them have not been proven to prevent or even slow down the progression of the disease. Therefore, it is imperative to develop safe and effective approaches to attenuate or halt the disease progression, or even reverse the disease through regeneration of new articular cartilage.

Microspheres are at the forefront of drug delivery and tissue engineering applications, displaying functions comparable to 3D scaffolds, which have already been harnessed for cell transplantation or drug/growth factor delivery at injury sites [5]. Microspheres can be injected into irregular defects or injured tissues in a minimally invasive procedure, thereby shortening the recovery time for up to several folds than that of the traditional surgical procedures as required for 3D scaffolds [6]. So far, microspheres displaying different types of shapes and structures, such as solid, hollow, and nanofibrous have been successfully fabricated. Of these, nanofiber microspheres exhibit large specific surface area, which endows them with high cell/drug loading efficiency. Ma *et al.* leveraged self-assembling star-shaped poly(l-lactic acid) (SS-PLA)-based nanofibrous microspheres for osteochondral repair [7]. Similarly, chitosan nanofiber microspheres were fabricated by using microfluidic device through physical gelation and exploited for the transplantation of chondrocytes for cartilage tissue engineering (CTE) [8]. Nonetheless, these platforms require the specific surface functional groups of materials, which may however be applicable to only a few polymers.

Recently, electrospinning combined with electrospraying technology has been leveraged for the production of nanofiber microspheres. This approach exploits homogenized electrospun nanofibers as raw ingredients, thereby avoiding the dense structure of the traditional electrospun nanofibers. The microstructure of nanofiber microspheres can be tailored by controlling different types of electrospraying parameters, such as applied voltage, flow rate, and spinneret-to-collector distance [9]. Besides, a series of materials, including both natural or synthetic polymers as well as inorganic oxides can be tailored into nanofiber microspheres [10,11]. Moreover, nanofiber microspheres not only display geometric compatibility, but may also be exploited for drug release due to their high specific surface area [12]. Nonetheless, the long-term mechanical stability of nanofiber microspheres requires further improvement. In addition, nanofibrous microspheres are needed to be further tailored for anti-oxidative properties, extracellular matrix (ECM) secretion, and chondrocytes protection to better satisfy the requirements for the OA treatment.

Polyphenols have been shown to exert anti-oxidative effect, which may not only neutralize harmful free radicals but also reduce cell apoptosis [13]. Tannic acid (TA) exhibits multiple pyrogallol hydroxyl groups, which afford reversible interactions with different types of the proteins, including gelatin and elastin through forming hydrogen bonds [14,15]. Besides, the adjacent hydroxyl groups in TA provide chelating sites that can be further reacted with different types of metal ions to afford 3D stable metal phenolic networks (MPNs) [16]. Moreover, TA exhibits high scavenging capacity for hydrogen peroxide (H_2O_2) and hydroxyl radicals (OH·) and promotes the release of glycosaminoglycans (GAGs) against

collagenase digestion. Therefore, the TA exhibits beneficial effects in protecting cartilage under OA conditions [17,18]. Strontium (Sr), an important trace element in the human body, has been widely used for the treatment of osteoporosis and has been shown to have a positive intervention on cartilage matrix remodeling [19–21]. Given the studies above, we hypothesized that the construction of strontium and TA mediated MPNs on nanofiber microspheres may enhance the bioactivity of microspheres and achieve the synergistic effect of antioxidant and chondrocyte anabolism to meet the requirements for OA therapy.

The objective of this study is therefore to design MPNs modified electrospray nanofiber microspheres and to evaluate their potential for OA treatment for the first time. Herein, we prepared gelatin/poly(L-lactide) (gelatin/PLA)-based nanofiber microspheres by electrospraying the aqueous dispersions of electrospun homogenized short fibers. The nanofiber microspheres were further modified with TA or TA/Sr^{2+} MPNs and were intensively characterized for morphological and physico-chemical characteristics, anti-oxidative ability, and drug/ion release. In addition, nanofiber microspheres were investigated in terms of anti-apoptosis, resolution of inflammatory cytokines as well as the secretion of cartilage-related ECM both *in vitro* and *in vivo* in an OA environment.

2. Materials and methods

2.1. Materials

Gelatin (Gel, 240 g Bloom) was purchased from Aladdin reagent Co., Ltd. (Shanghai, China). Poly(L-lactide) (PLA, M_W = 200 kDa) was purchased from Jinan Daigang Biomaterial Co., Ltd. (Jinan, China). Hexafluoroisopropanol (HFIP) was obtained from Shanghai Darui Fine Chemical Co., Ltd. (Shanghai, China). Tannic acid was supplied by Macklin Biochemical Co., Ltd. (Shanghai, China). Strontium chloride hexahydrate (SrCl$_2$·6H$_2$O) was obtained from Macklin Biochemical Co., Ltd. (Shanghai, China). Glutaraldehyde was obtained from Aladdin Bio-Chem Technology Co., Ltd. (Shanghai, China). The 2,2-diphenyl-1-picrylhydrazyl (DPPH) was purchased from Sinopharm Chemical Reagent Co. Ltd (Shanghai, China).

2.2. Preparation of short electrospun gelatin/PLA nanofibers

Gelatin and PLA were separately dissolved in HFIP; the concentration of gelatin and PLA was 12% and 8%, respectively. The gelatin solution and PLA solution were mixed in a ratio of 10:3 (v/v). The gelatin/PLA nanofiber membranes were fabricated by electrospinning. Briefly, the solution was loaded into a 10 mL syringe with a 20 G blunt-ended needle and pumped by a syringe pump at a flow rate of 3 mL/h with a voltage of 12 kV applied on the needle to afford electrospun membranes. The distance from the spinneret-to-collector was 15 cm. The gelatin/PLA nanofiber membranes were cross-linked by glutaraldehyde (GA) vapors from a 25% ethanolic solution for 6 h. Electrospun membranes were dried in a vacuum-oven at 37°C for up to three days. The cross-linked nanofiber membranes were then cut into small pieces (0.5 cm × 0.5 cm) and dispersed in water to afford 20 mg/mL dispersion. The uniform fiber dispersions were obtained by homogenizing with a probe homogenizer (IKA T18, Germany) for 10 min at 6000 rotations per minute (rpm). The well-homogenized nanofiber-dispersed solution was subsequently used for electrospraying.

2.3. Fabrication of gelatin/PLA-based nanofiber microspheres

The nanofiber microspheres, including gelatin/PLA-based nanofiber microspheres (MS), tannic acid-modified nanofiber microspheres (TMS) and tannic acid/Sr^{2+}-modified nanofiber microspheres (TSMS) were prepared by electrospraying method,

which was performed in the dripping mode [22]. Briefly, aqueous dispersion of short fibers (concentration, 20 mg/mL) was loaded into 10-mL syringe equipped with a 21G blunt-ended needle and pumped at a flow rate of 2.0 mL/h. A piece of aluminum (Al) foil was immersed in the liquid nitrogen as the ground collector for MS collection. The typical electrospray parameters were as follows: voltage = 8 kV and distance between the needle tip to collector/grounded electrode = 10 cm. After electrospraying, the frozen nanofiber MS were immediately transferred to a freeze dryer and lyophilized for 24 h. Subsequently, the MS were crosslinked by GA vapors in a closed chamber for 6 h to mechanically strengthen the particles and subsequently subjected to drying in a vacuum-oven at 37°C for 72 h. For the TMS, dried MS (weight, 50 mg) were immersed into 10 mL TA aqueous solutions (concentration, 3 mg/mL), and stirred for 10 min. After rinsing three times with the deionized water and freeze-drying, the dried TMS were obtained. For the TSMS, 50 mg MS were first immersed in the TA solution (concentration, 3 mg/mL) and stirred for 10 min, and then 1 mL of 0.1 M $SrCl_2 \cdot 6H_2O$ was added and microspheres were stirred for another 10 min. Thereafter, TSMS were obtained by lyophilization.

2.4. Characterization

The bright-field and fluorescence images of short fibers were collected by microscope (DMi 8, Leica, Germany). Image J (National Institutes of Health, Bethesda, MD) was used to measure the length of short fibers (n = 200) from 10 images. The morphology of short fibers as well as different microspheres was characterized by scanning electron microscopy (SEM, Phenom XL, Phenom Scientific Instruments Co. Ltd., Shanghai, China). Samples were mounted on an aluminum stub by using carbon tape and were sputter-coated with gold. Subsequently, the morphology of different samples was ascertained at an accelerating voltage of 10 kV. The SEM images were analyzed by using Image J software to measure the fiber diameter, pore size as well as diameter of different microspheres.

The elements on the surface of different microspheres were detected by an energy dispersive spectrometer (EDS, JSM-7500F, China). X-ray photoelectron spectroscopy (XPS, ESCALAB 250Xi, Thermo Fisher Scientific, Waltham, UK) was used to determine surface compositions of the different microspheres. For structural elucidation of different microspheres, Fourier transform infrared spectroscopy (FTIR) was performed by using a Nicolet-6700 FTIR spectrometer (Thermo Fisher Scientific, USA) in the range of 1900-600 cm^{-1}.

To evaluate the release kinetics of TA, 10 mg of different microsphere groups was immersed in 10 mL of phosphate buffered saline (PBS, pH 7.4) at 37°C. At appropriate intervals, the release media were removed, and the same volume of fresh media was added. The concentration of the TA in the release media was determined by UV/vis spectrophotometer (JASCO V530, JASCO, Japan) at 273 nm. To evaluate the release kinetics of Sr^{2+}, the supernatants of TSMS collected at different time intervals were analyzed by using inductively coupled plasma-atomic emission spectrometry (ICP-AES, Leeman, USA).

Total anti-oxidative capacity of microsphere extracts was measured by the 2,2-azino-bis-(3-ehylbenzothiazo-line-6-sulphonic acid) diammonium salt (ABTS) radical cation method [23]. Briefly, ABTS solution (7 mM) and potassium persulphate ($K_2S_2O_8$, 2.45 mM) were dissolved in deionized water and incubated at room temperature for 16 h in dark. The $ABTS^{\bullet+}$ solution was diluted with PBS to afford an absorbance value of 0.700 at 734 nm. Then, 0.15 mL of the extract solution collected from the microspheres at different time intervals (10 mg microspheres were immersed in 10 mL PBS for 24 and 48 hours, respectively to obtain the extract solution from the microspheres) was added to a total 2.85 mL of $ABTS^{\bullet+}$ solution. The solutions were allowed to mix at ambient

temperature in the dark for 6 min and the absorbance was measured at 734 nm. Ascorbic acid was used as a positive control. The radical scavenging activity (RSA) was calculated by Eq. (1):

$$\text{ABTS radical scavenging activity } (\%) = [(A_0 - A_1)/A_0] \times 100 \quad (1)$$

where A_0 and A_1 represent the absorbance of the control radical cation solution and the sample, respectively.

The anti-oxidative activity of different microspheres was further assessed by 2,2-diphenyl-1-picrylhydrazyl (DPPH) assay. Briefly, 2 mL of the extract solution of the microspheres collected at 24 and 48 hours was mixed with 2 mL of 0.1 mM DPPH/ethanol solution, while being protected from the light at room temperature. After reacting for 0.5 h, the absorbance of each mixture was measured at 517 nm by using ethanol as a blank. Pure ascorbic acid (AA) was used as a positive control, while DPPH solution without samples was used as a blank. Radical scavenging activity was calculated by Eq. (2):

$$A (\%) = (A_B - A_S)/A_B \times 100\% \quad (2)$$

where A indicated the DPPH· scavenging rate, while A_B and A_S indicated the absorbance of the blank and experimental groups, respectively.

For *in vitro* degradation assay, MS, TMS and TSMS were weighed in the dry state to record their initial weight (W_0). Thereafter, the microspheres were transferred into centrifuge tubes containing 10 mL of PBS (pH = 7.4 ± 0.1), which were placed in a thermostatic shaker at 37 °C with a speed of 100 rpm. On weekly intervals for up to eight weeks, the microspheres were removed, dried at room temperature, and weighed (W_1). The weight loss (W_L) was calculated by Eq. (3):

$$W_L = (W_0 - W_1)/W_0 \times 100\% \quad (3)$$

The microspheres were incubated in protease XIV solution (Concentration: 1.0 U/mL in PBS, Sigma, China) to evaluate degradation properties. Protease XIV has been shown to be much more effective in the digestion of the casein than that of the trypsin, chymotrypsin and several other proteases [24]. The samples were immersed into 10 mL enzyme solution with bath ratio of 1:10 (g/mL) and kept at 37°C in a shaking water bath. The degradation solution was refreshed every three days. After 1, 3, 7, 14, and 21 days, the samples were harvested and rinsed in deionized water for three times slightly. After freeze-drying, the ratio of degraded microsphere weight to initial weight was calculated as weight remaining (n = 3).

2.5. Biocompatibility of scaffolds in vitro

Articular cartilage was derived from New Zealand white rabbit (age, 4 months; weight, 2.5 kg) and chondrocytes were isolated as previously reported [25]. The acquired chondrocytes were cultured, and expanded in the culture medium (high glucose, Dulbecco's modified Eagle's medium (DMEM, Gibco, USA) supplemented with 10% fetal bovine serum (FBS, Hyclone, USA) and 1% penicillin/streptomycin/amphotericin B solution in an incubator at 37°C [26]. Chondrocytes at the second passage were used for the subsequent *in vitro* experiments. To investigate the effect of different microspheres on chondrocytes, the extract solution from microspheres was prepared. Briefly, 1 mg/mL of MS, TMS or TSMS were suspended in culture medium for up to 1 week, and the supernatants were collected to culture chondrocytes. The chondrocytes cultured with medium without the extract solution of the microspheres were used as a blank group.

The cell viability and cell proliferation were determined by using live/dead assay and cell counting kit-8 (CCK-8) assay (Beyotime, China). Chondrocytes (2.0×10^4 cells/well) were seeded into 48-well plates and cultured with the extract solution collected from

different microspheres for up to 1, 3, and 5 days in an incubator with humidified atmosphere of 5% CO_2 at 37°C (n = 3). At each time point, the medium was removed. Thereafter, 200 µL of medium with 10% CCK-8 reagent was added to each well and incubated for up to 2 h at 37°C. The absorbance was measured using a microplate reader (Multiskan MK3, Thermo Fisher Scientific, USA) at the 450 nm for 100 µL of supernatant per well. The viability of chondrocytes under H_2O_2 (0.4 mmol/L) exposure was determined with CCK-8. Chondrocytes (2.0×10^4 cells/well) were further seeded in 48-well plates and cultured with the extract solution collected from microspheres with or without 0.4 mmol/L H_2O_2 for 24 h, followed by the above procedure of the CCK-8 assay and the absorbance was measured at 450 nm using a microplate reader (Multiskan MK3, Thermo Fisher Scientific, USA). Live/dead assay was performed by using a live/dead staining kit (YeasenBiotech, China). Briefly, chondrocytes (2.0×10^4 cells/well) were seeded in 48-well plates and cultured with the extract solution collected from the microspheres with or without 0.4 mmol/L H_2O_2 for 24 h. After that, the medium was removed and the cells were incubated in PBS (100 µL) solution containing calcein-AM (5 µM) and propidium iodide (20 µM) for 15 min at 37 °C in the dark. The fluorescence of cells was observed by using a confocal laser scanning microscope (Nikon, A1RMP, Japan).

To gain an insight into the apoptosis, chondrocytes were cultured with the extract solution obtained from nanofiber microspheres under H_2O_2 treatment and were analyzed by TUNEL assay by following manufacturer's instructions (Beyotime, Shanghai, China). Chondrocytes (2.0×10^4 cells/well) were seeded along with the extract solution from various groups in a 48-well cell culture plate containing 0.4 mmol/L H_2O_2 for 24 h. Thereafter, cells were fixed with 1% paraformaldehyde for 10 min, followed by rinsing with the PBS three times. Then, cells were washed with 0.1% sodium citrate buffer solution and permeabilized with 0.1% Triton X-100 for 2 min, and washed three times with PBS. The cells were then incubated with the TUNEL staining solution (Beyotime, Shanghai, China) for 1 h, followed by staining with 4′,6-Diamidino-2-phenylindole (DAPI, Beyotime, Shanghai, China). The percentage of TUNEL-positive cells was calculated by counting the numbers of fluorescein-stained positive nuclei and normalizing with the total number of cells via Image J software.

The chondro-protective ability of different microspheres was further explored by real-time reverse transcription polymerase chain reaction (RT-PCR) analysis. Chondrocytes at a density of 5×10^5 cells/mL were seeded in a 6-well plate, treated with 0.4 mmol/L H_2O_2 and cultured with the extract solution of MS, TMS or TSMS for 24 h. The total mRNA of chondrocytes was collected by using TRIzol reagent (Invitrogen, Life Technologies, CA, USA), and cDNA was synthesized from 1 µg of collected RNA by using M-MLV cDNA Synthesis Kit (Promega, USA). Then, the cDNA was mixed with SYBR Green PCR Master Mix (TaKaRa, Kusatsu, Japan) and PCR was performed by using ABI StepOnePlus™ Real-Time PCR system (Applied Biosystems, USA). All primer sequences are listed in Table S1. The mRNA expression levels of tumor necrosis factor-alpha (TNF-α), aggrecan (ACAN), collagen II, matrix metalloproteinases-13 (MMP13), Adamalysin-like metalloproteinases with thrombospondin (TS) motifs (ADAMTS)-5, tachykinin1 (TAC1), and β-actin were quantified. The expression of all genes was normalized to β-actin as well as to the gene expression of chondrocytes without H_2O_2 treatment (control group) and the relative expression was calculated by $-2^{\Delta\Delta Ct}$ method.

To explore the moderating effect of different nanofiber microspheres on the inflammatory response, chondrocytes at a density of 0.5×10^5 cells/mL were seeded onto the coverslips in a 24-well cell culture plate and treated with 0.4 mmol/L H_2O_2. Thereafter, the extract solution obtained from different nanofiber micro-

spheres was added to the wells and samples were cultured for 24 h. Then the cells were fixed with 4% paraformaldehyde (15 min) and treated with 0.1% Triton X-100/PBS solution for 10 min, and 2% bovine serum albumin (BSA)/PBS mixture solution for 45 min. Afterwards, chondrocytes were incubated with anti-TNF-α antibody overnight (Abcam; 1:100 dilution) at 4°C. After PBS washing, chondrocytes were incubated with fluorescent-labeled secondary antibodies (Abcam; 1:200 dilution). DAPI was used to stain the cell nuclei for 10 min. Imaging was performed by using a fluorescence microscope (DMi 8, Leica, Germany).

2.6. Evaluation of nanofiber microspheres in an osteoarthritis model

All animal experiments were performed according to the standard guidelines approved by the ethics committee of Shanghai Jiao Tong University (SJTU). Adult healthy New Zealand white rabbits, (male; age, 4 months; weight, 2.5 kg) were randomly chosen and divided into three groups (n = 4 per group). The OA model was induced in the right knees of the rabbits by intra-articular injections of 500 µL of 4% papain solution [27]; all of the animals were injected with the papain solution once weekly for up to 4 weeks [28]. Afterwards, the OA rabbits received intra-articular injection of 50 µL of PBS, MS (10 mg/mL), TMS (10 mg/mL), or TSMS (10 mg/mL) once at first week after modeling. A sham group was conducted without OA induction. After four weeks of therapy, animals were euthanized and sacrificed. The joints were harvested for further examination. To evaluate the biosafety of different microspheres *in vivo*, the organs (heart, liver, spleen, lung, and kidney) were harvested, fixed in 4% paraformaldehyde and embedded in paraffin. Subsequently, tissue sections were stained with H&E and imaged under a microscope (DMi 8, Leica, Germany).

2.7. Articular cartilage regeneration in rabbits

The harvested knee joints were fixed, decalcified, paraffin embedded, and sectioned (5 µm). The H&E, Safranin O-fast green, collagen II and TNF-α were used to stain the sections for histological and immunohistochemical analysis. The relative expressions of collagen II and TNF-α were quantified by Image J software. The severity of the OA lesions was evaluated by using the OARSI (Osteoarthritis Research Society International) score established by Pritzker et al. [29], which scores the product of six grades (depth of lesion) and four stages (extent of involvement) on a scale of 0 (normal) to 24 (severe OA). A modified Mankin's histological score was used to score histological injuries of the articular cartilage [30], and the grading and scoring criteria are shown in the Table S2.

The TUNEL assay was used to determine the apoptosis of chondrocytes in the knee joints. The sections were fixed with 4% paraformaldehyde for 10 min, followed by incubation with acetic acid/ethanol mixture solution (1:2, v/v) for 5 min and rinsing with the PBS two times. Thereafter, the sections were incubated with the terminal deoxynucleotidyl transferase (TDT) in an incubator for 1 h at 37 °C. After TDT treatment, anti-digoxigenin conjugate (fluorescein) was added for 30 min, and the stained cells were preserved in mounting medium containing DAPI (Beyotime, Shanghai, China). The percentage of TUNEL-positive cells was calculated by counting the numbers of fluorescein-stained positive nuclei and normalizing them with the total number of nuclei via Image J software.

To further observe inflammatory response of the joint cartilage, sections were stained with interleukin-1 beta (IL-1β). Rehydrated sections were incubated with trypsin antigen solution at 37°C for 15 min, followed by incubation with 3% H_2O_2 for 15 min at room temperature to block the endogenous peroxidase. After

blocking with 10% normal goat serum, the sections were incubated with anti-IL-1β antibody (Abcam; 1:200 dilution) at 4°C overnight. Next, the sections were incubated with fluorescent-labeled secondary antibody (Abcam; 1:200 dilution) for 1 h and finally counterstained with DAPI. The fluorescence intensity was quantified by image J software. The synovial fluid was also collected by using a 2 mL syringe with an 18-gauge needle and centrifuged at 4000 rpm for 20 min at 4°C. The supernatant was collected and frozen at -80°C. The H_2O_2 levels were measured through a hydrogen peroxide assay kit (Beyotime, Shanghai, China) following the manufacturer's instructions. The IL-1β was measured by using the rabbit IL-1β enzyme-linked immunosorbent assay (ELISA) kit (Solarbio, Beijing, China) according to the manufacturer's instructions. The concentrations of osteoprotegerin (OPG) and receptor activator of nuclear factor κB ligand (RANKL) were both measured by ELISA reagents (Boster, Wuhan, China). The ELISA tests were performed according to the manufacturer's instructions. The optical density was measured at 450 nm by using a microplate reader (Multiskan MK3, Thermo Fisher Scientific, USA).

2.8. Statistical analysis

Quantitative data were expressed as mean ± standard deviation (SD). Origin 8.0 (origin Lab Inc, USA) was applied for helping statistical analysis. For statistical significance, one-way analysis of variance (ANOVA) with Tukey's post-hoc test was performed. A p value < 0.05 was considered to be statistically significant.

3. Result

A schematic diagram summarizing the fabrication process of NF microspheres was shown in Fig. 1. Short fiber segments were obtained from electrospun nanofibers through an ultrasonic homogenizer. The homogenized fibers were electrosprayed into liquid nitrogen, and then freeze-dried and cross-linked to obtain mechanically stable microspheres. Subsequently, MS were immersed into a mixture solution of TA and $SrCl_2$. In previous studies, MPNs coatings on biomaterials were formed by different methods, such as hydrogen bonding, cationic-π interactions and π-π stacking of catechol and gallol groups [31]. The catechol groups of TA exhibit multiple sites for hydrogen and coordination bonding. It is therefore reasonably expected that these types of interactions may be responsible for the formation of TA-based MPNs on the microspheres.

The freeze-dried short fibers were uniformly distributed in water, and the homogenized short fiber dispersion was easily extruded through a syringe equipped with a blunt-ended needle (Fig. 2A-D). The fluidity of short fiber dispersion was crucial for the subsequent electrospray process, because it can avoid the obstruction of the needle for efficient production of microspheres. Fig. 2E-F revealed the bright field and fluorescence photographs of gelatin/PLA short nanofibers upon cross-linking with GA vapors. SEM micrographs of homogenized nanofibers were shown in Fig. 2H-I. After homogenization, nanofibers displaying relatively short and uniform length could be clearly observed from SEM
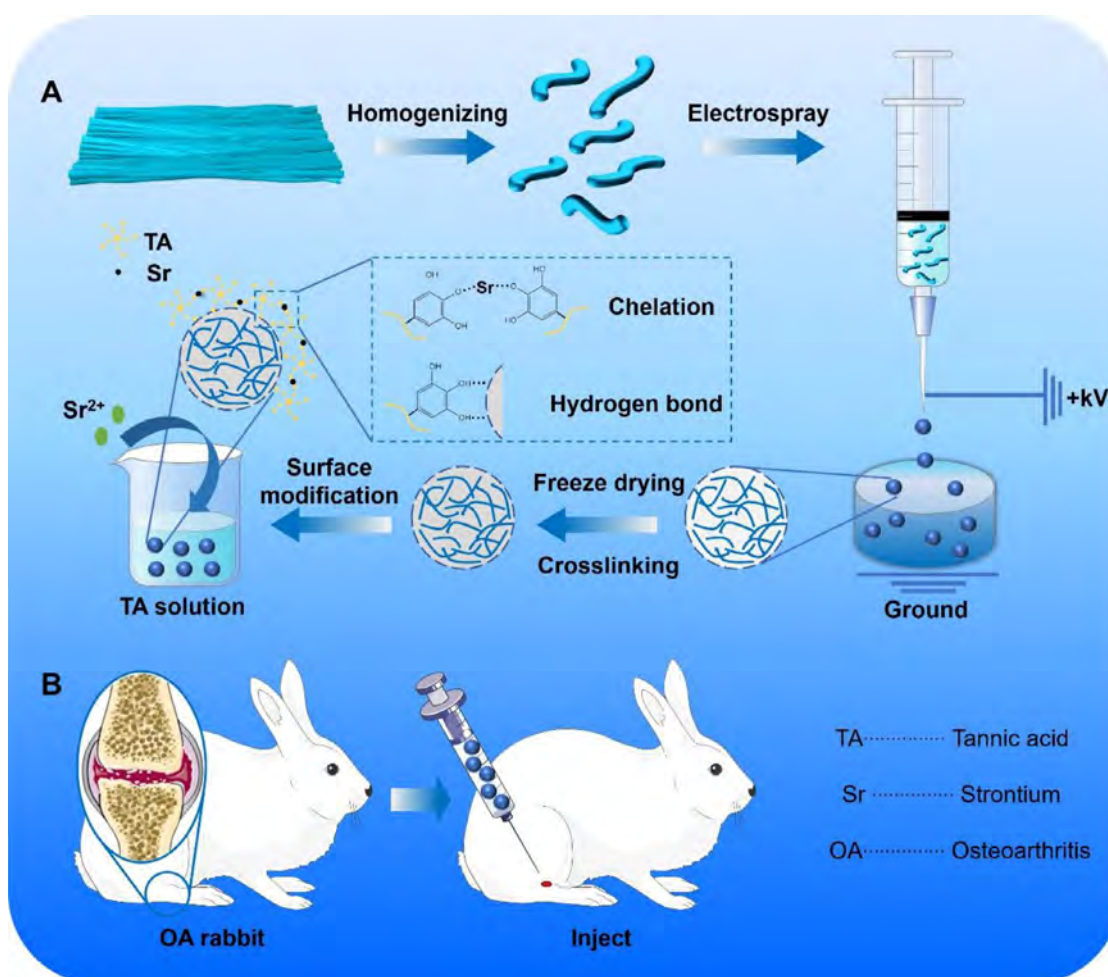
Fig. 1. Fabrication and application of nanofiber microspheres. (A) Schematic diagram illustrating the fabrication process of microspheres and the mechanism for the modification of microspheres with TA or TA/Sr^{2+}. (B) Intra-articular injection of microspheres in an OA model of rabbit.
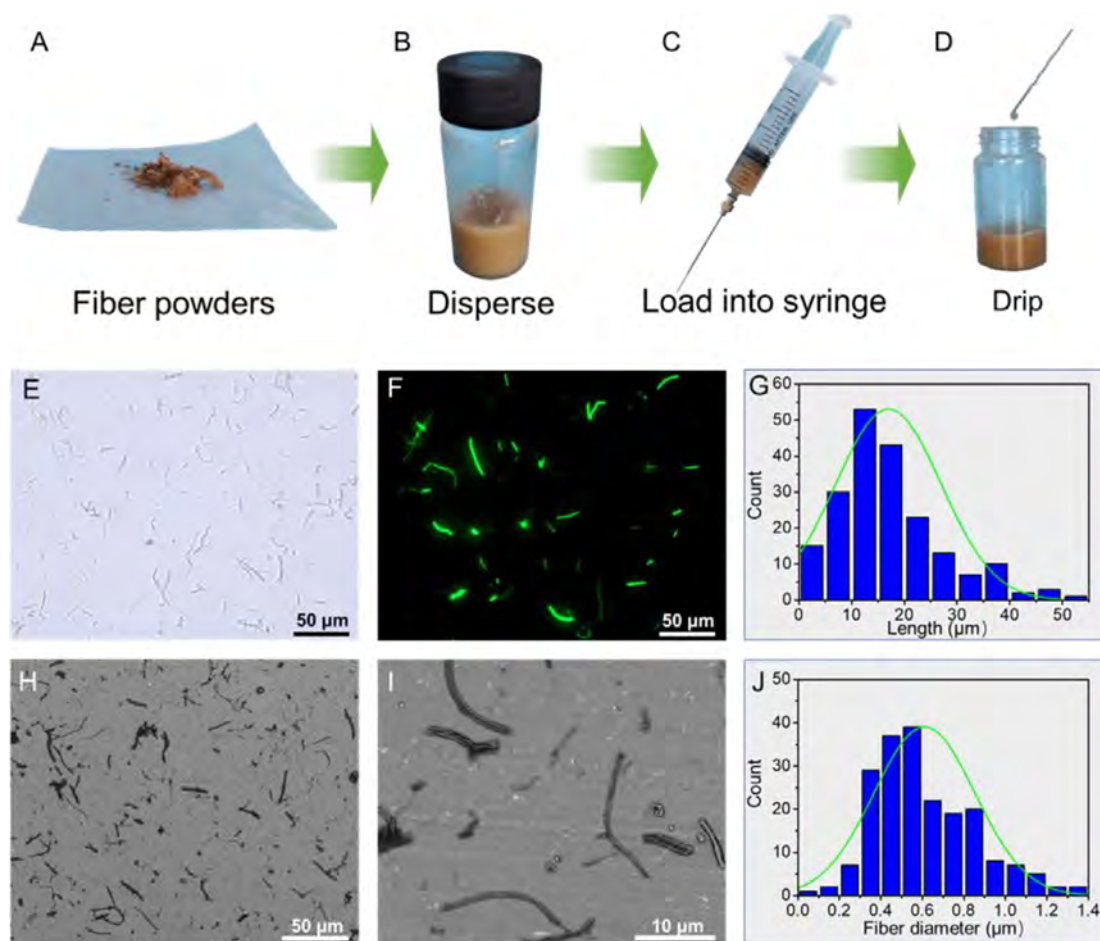
Fig. 2. Morphological analysis of short nanofibers. Photographs of homogenized lyophilized nanofibers (A), short nanofibers dispersed in water (B), homogenized short nanofibers loaded into a syringe (C) and short nanofibers extruded through a stainless steel needle (D). The bright field (E), fluorescence (F) and SEM (H-I) images of homogenized nanofibers. Length (G) and fiber diameter (J) distribution of homogenized nanofibers (n = 200).

micrographs. The length and diameter distributions of nanofibers were shown in Fig. 2G & J, respectively. After homogenization, the length of short fiber segments was 17.01 $\pm$ 10.02 µm, while the average diameter of the short fiber was 610 $\pm$ 244 nm.

The morphology of MS, TMS, TSMS microspheres was shown in Fig. 3A & S1. All of the microspheres displayed biomimetic nanofibrous surface topography. Moreover, thin strips were formed on the surface of the microspheres which became more evident after the introduction of Sr^{2+}. Morphological examination of the nanofiber segments at high magnification further revealed that some small particles of TA were distributed on the fiber surface of TMS and TSMS. It was worth noting that the microspheres without crosslinking with the GA vapors demonstrated poor mechanical stability and were prone to be collapsed (Fig. S2). Quantitative analysis revealed an insignificant difference among MS, TMS, TSMS in terms of the fiber diameter and pore size (Fig. 3B-C). Nonetheless, the diameter and pore size of the microspheres were slightly decreased after treatment with the TA, which may be ascribed to the polyphenol-mediated crosslinking of microspheres as well as the introduction of Sr^{2+}, which may lead to the formation of coordination bonds and further strengthen the inter-fiber linkages.

Energy-dispersive spectroscopy (EDS) as well as elemental analysis of microspheres demonstrated the uniform distribution of elements, including C, O, N, and Sr in TSMS microspheres (Fig. 4D). Quantitative analysis further showed a reduction in C/O atomic ratio from 2.87 in the MS to 2.24 in the TMS and 1.79 in the TSMS after coating with TA. These ratios were close to the atomic ratio

of TA (1.24) (Table S3). The XPS spectra further illustrated an interaction between the MS substrate and the TA-Sr coating. While MS and TMS were devoid of the Sr 3d spectrum, the TSMS exhibited Sr 3d spectrum (Fig. 3E & G). The O 1s spectrum in TMS and TSMS showed a higher bond energy (533.4 eV) than that of the MS group (531.7 eV), which corresponded to the oxygen in the phenolic groups of the TA on the microspheres, thereby indicative of the successful modification of the MS with the TA moieties (Fig. 3F).

The ATR-FTIR spectra of the TA, MS, TMS, TSMS were shown in Fig. 4H. For the pure TA, a characteristic peak at 1704 cm^{-1} was apparent due to the stretching vibrations of C=O (carboxylic ester) groups, and peaks at 1607, 1526, and 1445 cm^{-1} were consistent with the aromatic C-C stretches. Peaks at 1174 and 1021 cm^{-1} were attributed to vibrations of substituted benzene rings, while those at 1310 and 751 cm^{-1} were attributed to the out-of-plane and in-plane vibrations of O-H bonds, respectively [32]. MS spectrum displayed two distinctive peaks at around 1647 cm^{-1} and 1540 cm^{-1}, which were ascribed to the C=O stretching of the amide I as well as N-H bending and C-H stretching of amide II in the gelatin, respectively. The absorption peaks at 1758, 1452, 1183, 1130, and 1087 cm^{-1} corresponded to the C=O stretching vibration, -CH$_3$ stretching vibration, C-O stretching vibration, C-O-C stretching vibration, and C-O symmetric stretching in PLLA [33]. For the TMS and TSMS, in addition to the characteristic peaks possessed by MS, there were additional characteristic peaks at 1704, 1310, 1174, 1021 and 751 cm^{-1}, all of which were attributed to TA,
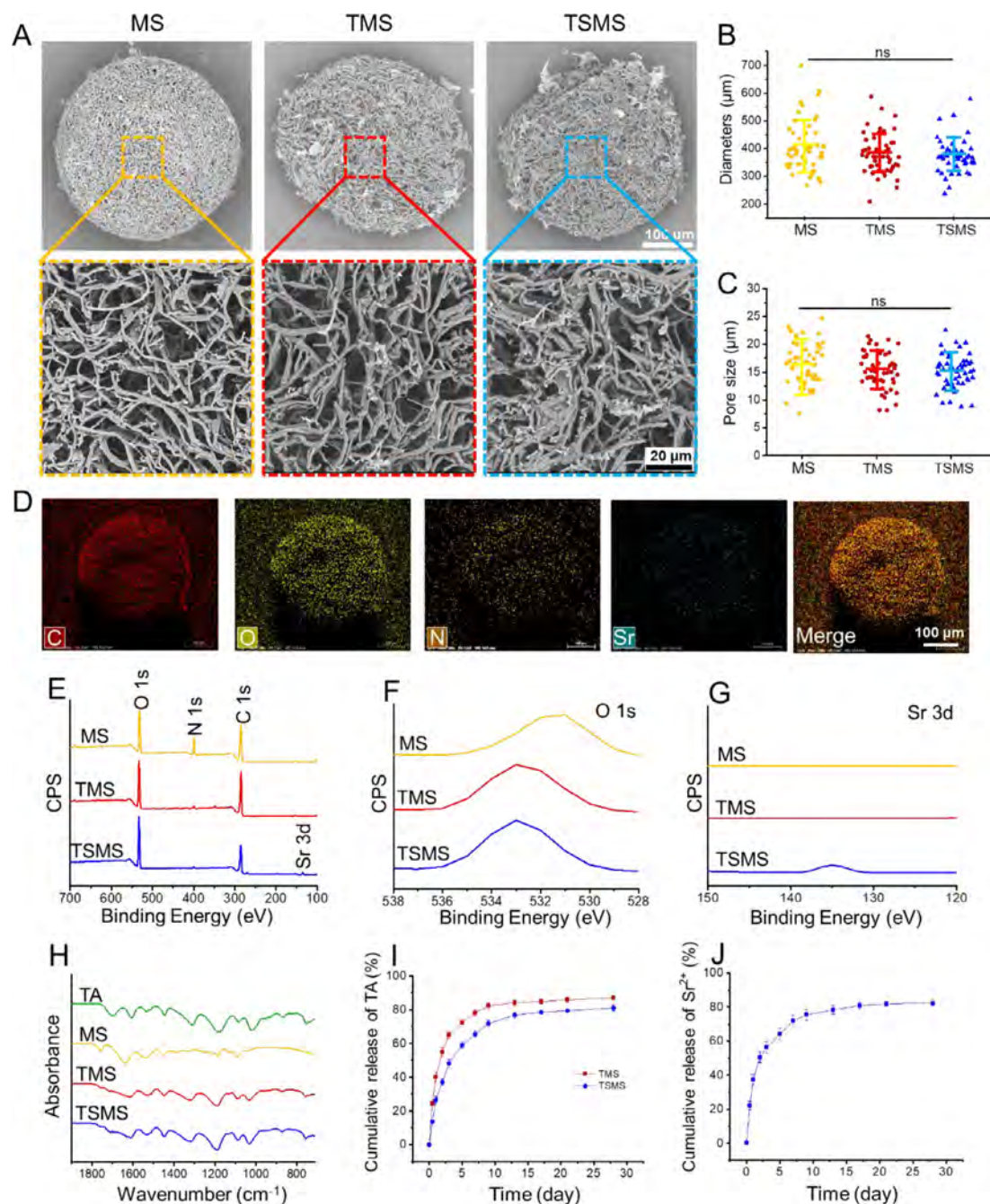
Fig. 3. Structural and morphological analysis of nanofiber microspheres. (A) SEM photographs of MS, TMS and TSMS. Diameter (B) and pore size (C) of different microspheres. (D) Representative elemental mapping of the TSMS. The XPS spectra of microspheres (E), high-resolution O 1s core level XPS spectra (F) and high-resolution Sr 3d core level XPS spectra (G) of MS, TMS and TSMS. (H) ATR-FTIR spectra of TA, MS, TMS and TSMS. (I) Release of TA from different microspheres in PBS at 37℃ (n = 3). (J) Release of Sr^{2+} from the TSMS incubated in PBS at 37 ℃ (n = 3).

with specific representative groups as discussed in the above paragraph. Conclusively, FTIR result illustrated the successful modification of TA on TMS and TSMS.

The results of TA release detected over 28 days were shown in Fig. 3I, where TMS exhibited a burst release at an initial stage. The TA was released for up to 40.24% in the first day of TMS and most of the residual drug was released in the following 9 days (accumulative release about 82.25%). Contrarily, the TSMS displayed sustained release of TA, with an initial fast release (26.63% on the first day), followed by a cumulative release of 78.55% within 14 days. Fig. 3J showed the release behavior of Sr^{2+} in TSMS, with the release rate of the ions being higher at the initial stage reaching for

up to 37.3% by first day. The total release of Sr^{2+} reached for up to 82.38% by day 28.

The degradation of the microspheres was further evaluated for up to 8 weeks *in vitro*. The weight loss was found to be 59.3 ± 3.5%, 65.3 ± 2.1%, and 61.3 ± 1.5% for MS, TMS, and TSMS after 8 weeks, respectively (Fig. S3). While there was an insignificant difference among different microspheres in terms of the weight loss over 8 weeks, the degradation rate of the TA-modified microspheres was faster than that of the MS group beyond week 6. The fast degradation of microspheres after 6 weeks may be ascribed to the release of TA, which may alter the pH, thereby accelerating the degradation [34,35]. As shown in Fig. S4, after 3 weeks exposure to
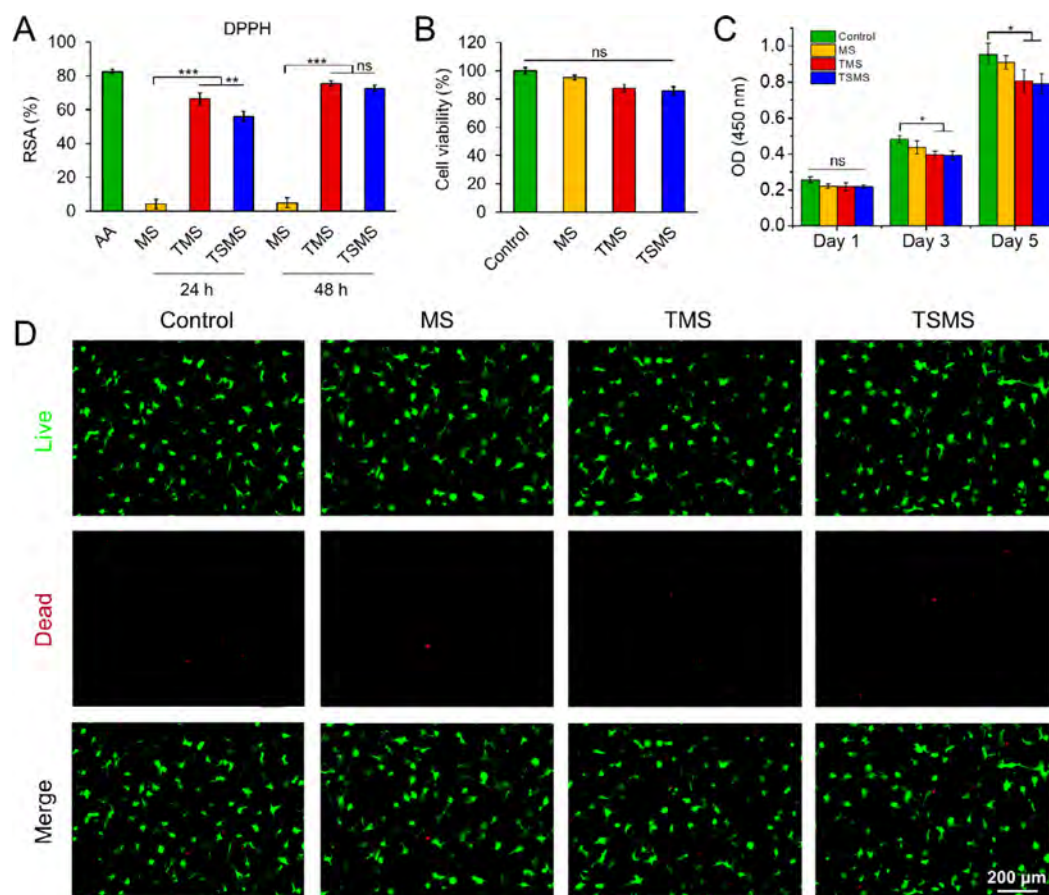
Fig. 4. Anti-oxidative ability and biocompatibility of microspheres *in vitro*. (A) Free radical scavenging capacity of MS, TMS, TSMS and AA determined by DPPH assay (n = 3). (B) Cell viability of chondrocytes co-cultured with the leachate of MS, TMS and TSMS for up to 24 h (n = 3). (C) Proliferation of chondrocytes co-cultured with the leachate of MS, TMS and TSMS at day 1, 3, and 5 (n = 3). (D) Live/dead assay of chondrocytes co-cultured with the leachate of MS, TMS, and TSMS for 24 h (live and dead cells have been stained in green and red colors, respectively).

protease XIV solution, weight loss of the MS group exceeded 78%, while those for the TMS and TSMS groups reached for up to 83% and 82%, respectively. Since the gelatin is the main component of the nanofibrous microspheres, the main degradation products are mainly free amino acids, which can be easily metabolizable *in vivo* [36]. On the other hand, the PLA is known to mainly undergo hydrolysis; the degradation products of the PLA can also be easily excreted by the metabolic pathways from the human body [37]. Though the content of TA and strontium ions are minute in the microspheres, Sr ions are mainly metabolized through urine *in vivo* [38]. The degradation products of the TA mainly consist of glucose and gallic acid, which are easily absorbed *in vivo*; the intake of a small quantity of TA has also been shown to be beneficial for the health [39].

The antioxidative activities of different microspheres were evaluated by using DPPH and ABTS assays. As shown in Fig. 4A, the MS did not exhibit an obvious free radicals scavenging activity both at 24 h and 48 h. On the other hand, TMS and TSMS showed significant scavenging effects on free radicals, and the radical scavenging capacity of these modified microspheres was increased with an increase in the incubation time. In the DPPH assay, the free radical inhibition rate was 66.43% and 75.45% for the TMS, while 56.01% and 72.58% for the TSMS group at 24 h and 48 h, respectively. On the other hand, in the ABTS assay (Fig. S5), the inhibition of free radicals of TMS was 73.08% and 81.34%, while 60.21% and 79.82% for the TSMS group at 24 h and 48 h of incubation, respectively.

The bioactivity of the different groups of nanofiber microspheres was next evaluated. There was no significant difference

among four groups in terms of the cell proliferation and cell viability within the first 24 h (Fig. 4B). As can be seen from Fig. 4C, the TMS and TSMS groups showed less cell proliferation than that of the control groups both at day 3 and day 7. Live/dead assay indicated minimal cell toxicity in all of the groups (Fig. 4D). Overall, these results revealed the free radical scavenging capacity and good cytocompatibility of the TA-modified microspheres.

In this study, we used H_2O_2 to simulate the inflammatory microenvironment in the pathogenesis of OA. Live/dead cell assay indicated H_2O_2-mediated reduction in the numbers of live cells (shown in green color), while an increase in the numbers of dead cells (shown in red color) in each group than that of the non-treated control group (Fig. 5A). Chondrocytes co-cultured along with the leachate of TMS and TSMS showed only a few numbers of dead cells than that of the blank and MS groups (Fig. 5C). While H_2O_2 treatment significantly decreased the cell viability in all groups, the TMS and TSMS groups still showed higher cell viability than that of the blank and MS groups, indicating that the TA released from TMS and TSMS groups may effectively resist H_2O_2-induced oxidative stress (Fig. 5D). Furthermore, TMS and TSMS groups were able to protect the chondrocytes from the H_2O_2-induced apoptosis (Fig. 5B). Quantitative analysis also revealed the lower percentages of TUNEL-positive nuclei in TMS and TSMS groups (13% and 11% for TMS and TSMS, respectively). On the other hand, the percentage of TUNEL-positive nuclei was 46% and 41% in the blank and MS groups, respectively (Fig. 5E).

The expression level of TNF-α was detected by immunofluorescence staining (Fig. 6A). The fluorescence signal of TNF-α was sig-
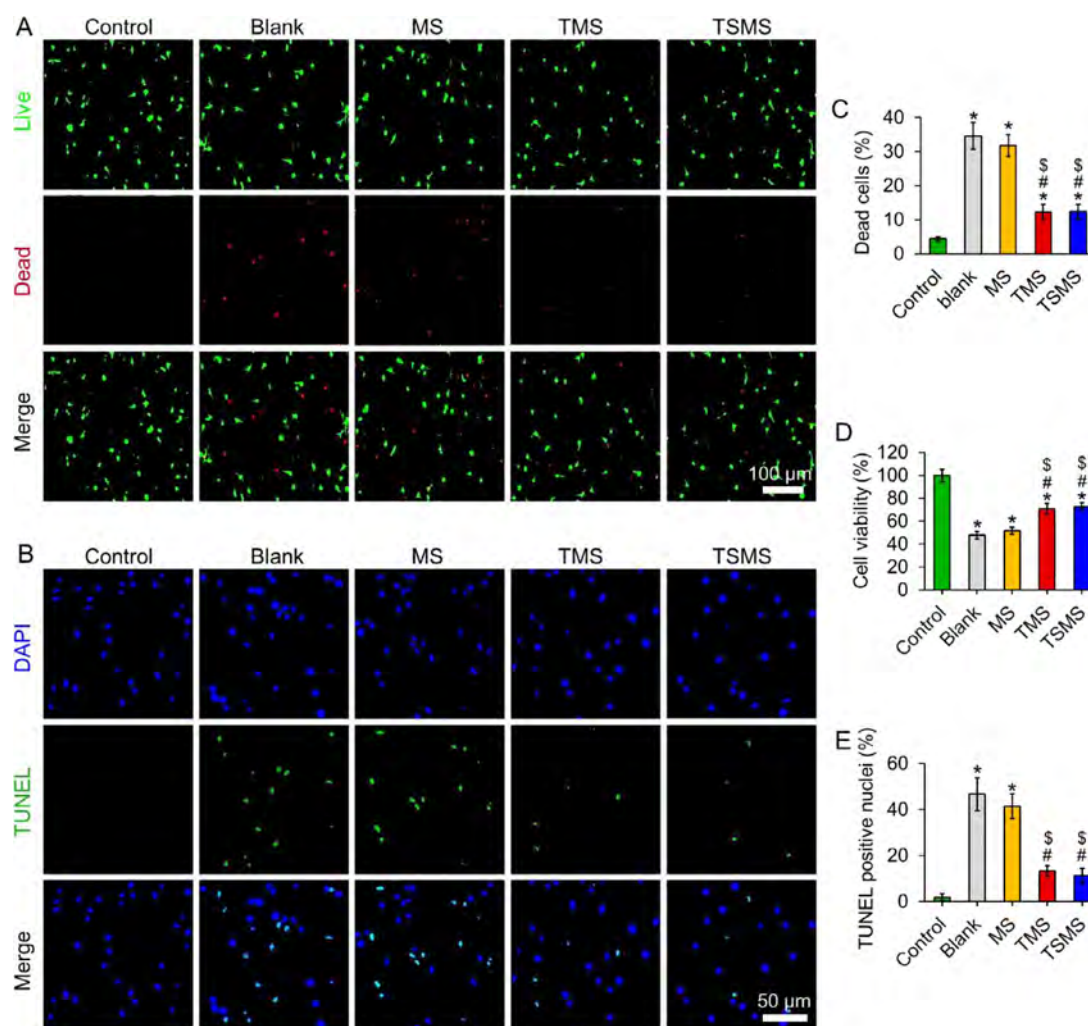
Fig. 5. Cytocompatibility of nanofiber microspheres in an oxidative environment *in vitro*. (A) Fluorescence images of chondrocytes co-cultured with the leachate of MS, TMS and TSMS after H_2O_2 treatment for 24 h. Green and red colors indicate live and dead cells. (B) TUNEL assay of chondrocytes cultured with the leachate of MS, TMS and TSMS after treatment with H_2O_2 for 24 h. (C) Percentage of the dead cells obtained from the live/dead staining assay (n = 3). (D) Cell viability of chondrocytes co-cultured with the leachate of MS, TMS and TSMS as detected by CCK-8 assay after H_2O_2 treatment for 24 h (n = 3). (E) Percentage of TUNEL-positive cell nuclei based on TUNEL assay (n = 3). (*, #, $, % indicate p < 0.05 as compared to the control, blank, MS, and TMS, respectively.)

nificantly increased after H_2O_2 treatment. Both the TMS and TSMS groups were more effective in reducing the fluorescence intensity of TNF-α than that of the blank and MS groups (Fig. S6). The TNF-α, ADAMTS5 and MMP 13 are reported to be involved in the degeneration of the cartilage matrix in the OA [40,41], while TAC1, a neuropeptide, is associated with the pain signaling [42]. The treatment of chondrocytes with the H_2O_2 effectively increased the mRNA expression levels of TNF-α, MMP13, ADAMTS5, and TAC1. As it was anticipated, the TMS and TSMS groups markedly reduced the expression levels of these genes as compared to the blank and MS groups (Fig. 6B-D & G). Typically, collagen II and aggrecan are abundantly expressed in the healthy chondrocytes. The RT-qPCR results showed that the TMS and TSMS groups could reverse the decreased mRNA expression levels of collagen II and aggrecan. The MS had only a limited effect on increasing the mRNA expression levels of collagen II and aggrecan, which were similar to that of the blank group (Fig. 6E-F). Moreover, the higher expression of ECM-related genes was detected in TSMS groups compared to the TMS groups, indicating the superiority of the strontium ions released from TSMS in promoting the production of cartilage matrix under OA condition.

After four weeks of the intra-articular injection of MS, TMS, and TSMS in an OA-induced rabbit model, the macroscopic appearance of the knee joints showed distinct histological features. The PBS and MS groups exhibited OA erosions and large lesions than that of the sham-operated group which displayed a glistening joint surface. Contrarily, in the TMS and TSMS groups, the joint surface was smooth, showing the mild OA, and the features of joints were similar to that of normal articular cartilage.

To gain a further insight into the cartilage degeneration and repair, histological analysis was performed by using H&E and Safranin O-fast green staining, while immunohistochemical analysis was carried out by using collagen II and TNF-α. As shown in Fig. 7A, the PBS and MS groups exhibited obvious morphological changes accompanied with the loss of the cartilage matrix, fissures and fibrillation. In contrast, TMS and TSMS groups exhibited morphology and tissue cellularity closely resembling the sham-operated group. The TSMS groups showed more deposition of collagen II, while a weak staining for TNF-α, which were similar to the sham groups, while strikingly different than that of the PBS, MS and TMS groups. On the other hand, both the PBS and MS groups displayed only a mild deposition of collagen II while
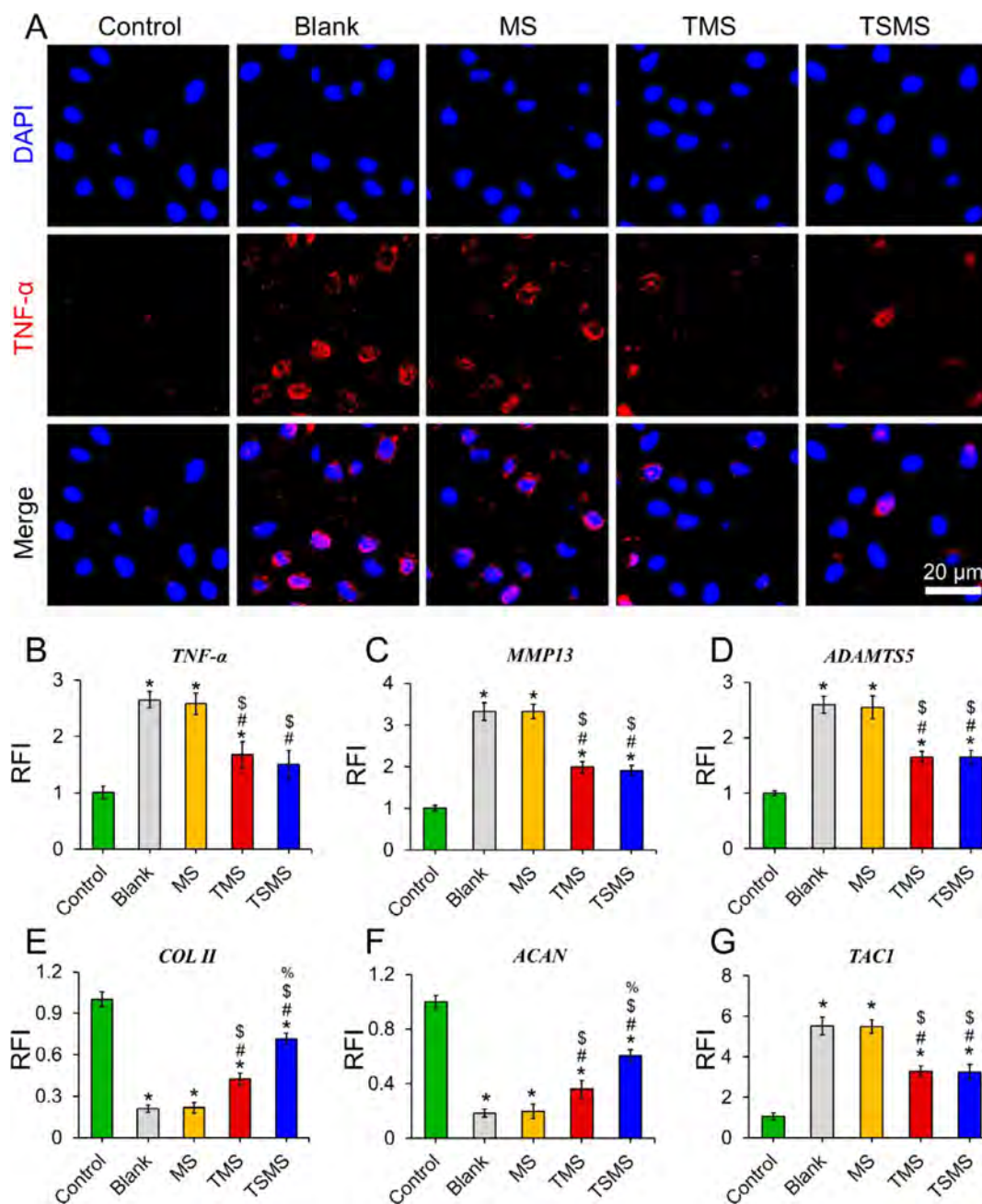
Fig. 6. Anti-inflammatory properties of nanofiber microspheres *in vitro*. (A) Fluorescence images showing the expression of TNF-α in chondrocytes treated with H_2O_2 and co-cultured with the leachate of MS, TMS, and TSMS for 24 h. The mRNA expression level of TNF-α (B), MMP13 (C), ADAMTS5 (D), collagen II (E), aggrecan (F) and TAC1 (G) in chondrocytes treated with H_2O_2 and co-cultured with the leachate of MS, TMS, and TSMS for 24 h. RFI = Relative fold induction. (*, #, $, % indicate p < 0.05 when compared with control, blank, MS, TMS, respectively.)

substantially stronger staining for TNF-α than that of TA-modified groups.

To evaluate the quality of the regenerated cartilage, the results of OARSI macroscopic score (a total 24 points), and Mankin score (a total 14 points) were summarized. The TSMS groups showed the lowest OARSI macroscopic score (7.0 ± 2.5) compared with the PBS (17.2 ± 2.2), MS (15.0 ± 2.4) and TMS groups (8.2 ± 1.7) (Fig. 7B). Mankin score further indicated a good repair outcome in TSMS group (2.75 ± 0.5) than that of the PBS (9.5 ± 0.5), MS (8.75 ± 0.5) and TMS groups (5.5 ± 1.0) (Fig. 7C). Furthermore, collagen II and TNF-α expressions were analyzed. The TSMS groups exhibited significantly higher expression levels of collagen II (0.66 ± 0.08 fold) than that of the PBS (0.26 ± 0.06 fold), MS (0.31 ± 0.05 fold) and TMS (0.50 ± 0.05 fold) groups (Fig. 7D). On the other hand,

the TNF-α expression level was found to be significantly less in the TSMS groups (2.91 ± 0.41 fold) than that of PBS (5.50 ± 0.43 fold), MS (5.33 ± 0.47 fold), and TMS (3.83 ± 0.43 fold) groups (Fig. 7E).

In vivo biosafety of different types of microspheres was further discerned by H&E staining of the major organs (heart, liver, spleen, lung, and kidney). The results showed an insignificant inflammation and no histological anomalies among the groups which were treated with the different types of microspheres compared to the sham group, thereby indicating a good *in vivo* biosafety of the microspheres (Fig. S7). Overall, these results indicate good biosafety of different types of microspheres, and the superiority of TSMS in alleviating inflammation and promoting cartilage matrix secretion in the OA microenvironment *in vivo*.
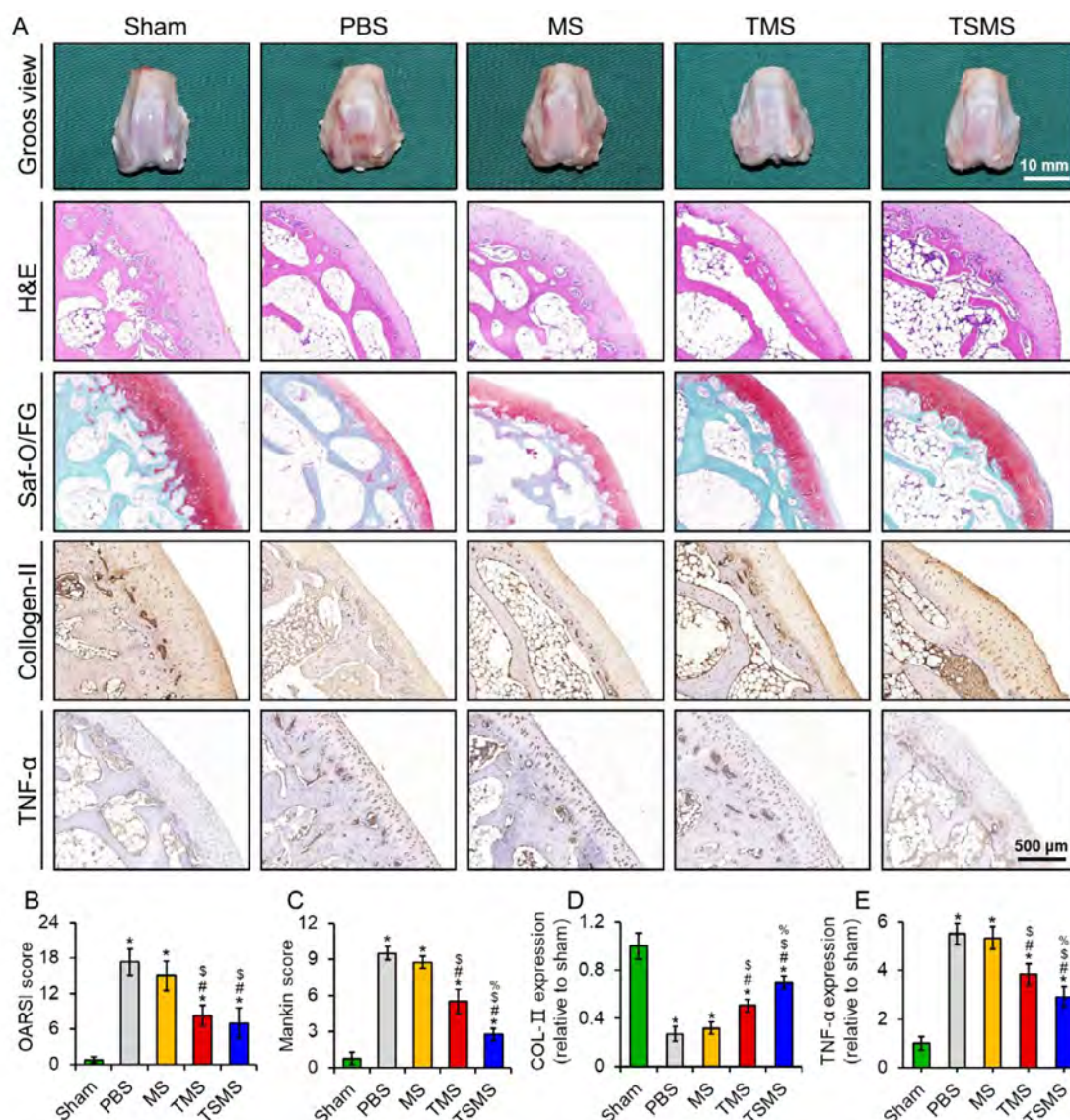
Fig. 7. Attenuation of the OA by different microspheres *in vivo*. (A) Macroscopic observations, H&E staining, Safranin O-fast green staining, collagen II, and TNF-α immuno-histochemical staining to evaluate therapeutic potential of microspheres in an OA model in rabbits for 4 weeks. OARSI score (B) and Mankin score (C) of the repaired tissue (n = 4). Quantification of the relative expression of collagen II (D) and TNF-α (E) (n = 4). (*, #, \$, % indicate p < 0.05 when compared with sham, PBS, MS, TMS, respectively.)

The apoptosis of articular chondrocytes *in vivo* was evaluated by TUNEL staining. As shown in Fig. 8A, TMS and TSMS groups displayed weak fluorescence expression of TUNEL-positive chondrocytes. In contrast, PBS and MS groups exhibited more fluorescence expression of TUNEL-positive chondrocytes. Quantitative analysis showed that the percentage of TUNEL-positive cells was significantly decreased in the TMS (18%) and TSMS (17%) groups than that of the PBS (41%) and MS groups (40%) (Fig. 8B). Intra-articular inflammatory response was further ascertained by immunofluorescence staining for IL-1β. In comparison to the PBS and MS groups, the TMS and TSMS groups showed weak fluorescence expression for IL-1β (Fig. 8C), which was further confirmed by the quantitative analysis of the fluorescence intensity and ELISA (Fig. 8D-E). While there was an insignificant difference between TMS and TSMS in terms of the numbers of the TUNEL-positive nuclei as well as IL-1β-positive expression, these groups exhibited significantly less numbers of TUNEL-positive nuclei as well as IL-1β-positive expression compared with the PBS and MS groups. In addition, the TA-modified microspheres demonstrated enhanced anti-oxidative effects to scavenge H_2O_2, thereby showing their superiority in eliminating the ROS *in vivo* (Fig. S8). An obvious

chondro-protective and anti-inflammatory effect of TSMS may be attributed to the sustained release of the TA from TSMS. The concentration of OPG and RANKL in synovial fluids was also determined and shown in Fig. S9. The TSMS group showed significantly higher levels of OPG than that of the PBS, MS and TMS groups. On the other hand, the TA-modified microspheres exhibited lower levels of RANKL while higher ratio of OPG/RANKL than that of the PBS and MS groups. Taken together, these results indicated that the TA-modified microspheres were superior in reducing cell apoptosis as well as alleviating inflammation in an OA model *in vivo*.

Fig. 9 showed the possible mechanism of MPNs-modified nanofiber microspheres in articular cartilage protection. Upon an injection of the microspheres into the joints, the MPNs on the microspheres may disintegrate and release TA and Sr^{2+} ions. The TA can scavenge free hydroxyl radicals (OH·) via the resonance stabilization of its phenolic π-electrons with the catechin and gallol groups, thus suppressing the expression of inflammatory factors and reducing the apoptosis. On the other hand, the Sr^{2+} ions replenish the concentration of cations in the joint and promote the secretion of cartilage specific matrix. These synergistic func-
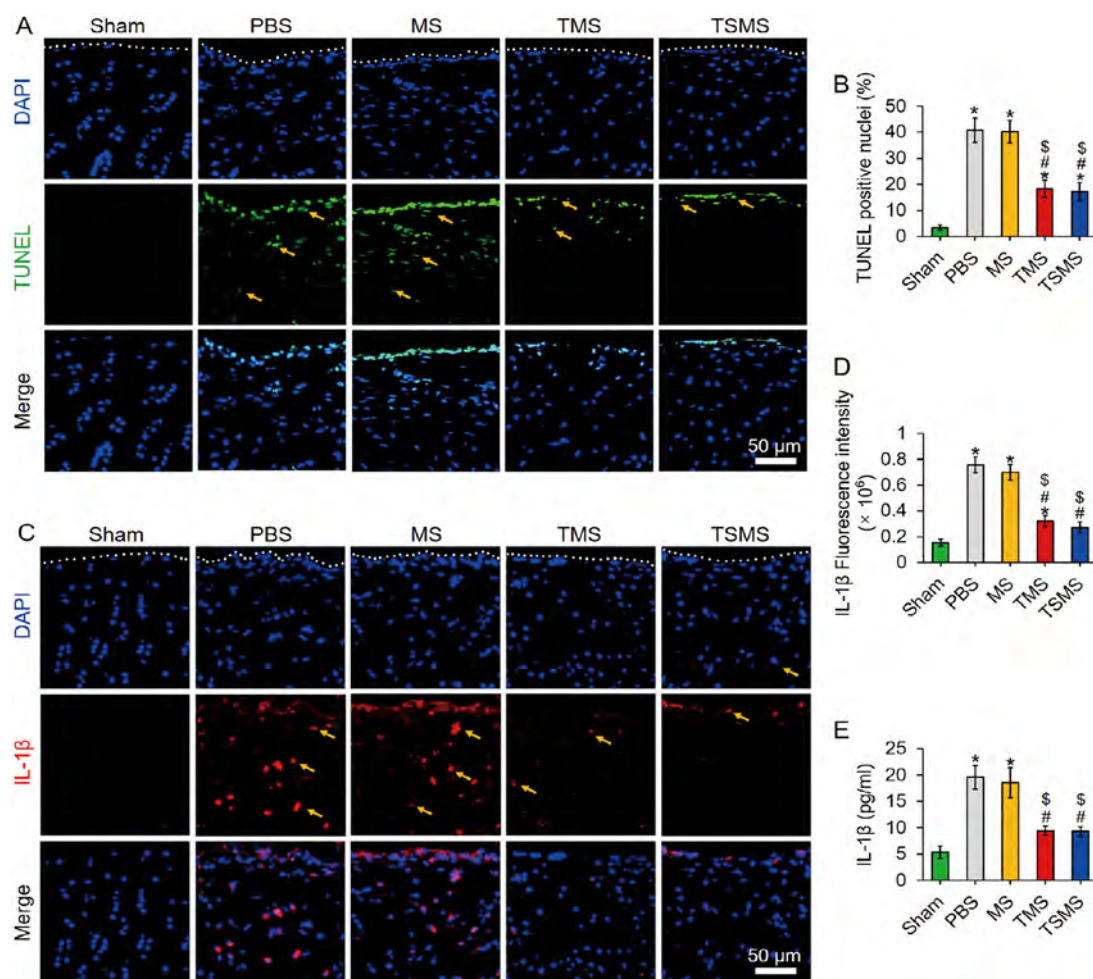
Fig. 8. Chondro-protective and anti-inflammatory effects of nanofiber microspheres *in vivo*. (A) Apoptosis of articular chondrocytes as revealed by TUNEL assay. (B) Percentage of TUNEL-positive cell nuclei (n = 3). (C) Inflammatory response characterized by immunofluorescent staining for IL-1β. (D) Fluorescence intensity of IL-1β (n = 3). The white dotted lines point toward the surface of articular cartilage. (E) Quantification of concentration of IL-1β in the joint fluid by using ELISA (n = 3). (*, #, $, % indicate p < 0.05 when compared with sham, PBS, MS, TMS, respectively.)

tions confer the TSMS with the reparative functions to alleviate osteoarthritis and protect cartilage degeneration.

4. Discussion

3D porous scaffolds have been developed for the regeneration of different types of tissues, including bone, cartilage, and skin due to their ECM-mimetic morphology and structural features [43–45]. The 3D injectable porous microspheres may facilitate minimally invasive filling of the irregular-shaped defects as well as promote tissue regeneration. Herein, we demonstrated the preparation of nanofiber microspheres and validated their potential for OA treatment in a rabbit model. Notably, the minimal invasiveness of injectable nanofiber microsphere may perhaps be a good alternative to the macroscopic 3D scaffolds, which often require open surgical procedures [46]. Electrospinning as a versatile nanofiber preparation technique has been realized by using a myriad of natural and synthetic materials and shown to be superior in terms of tailoring the morphological features of the scaffolds. While considerable research has been pursued on the deployment of 3D porous scaffolds for CTE, only a little research has been carried out on electrospun scaffolds for OA treatment. Ansari et al. [47] developed dexamethasone-loaded nanofibrous PLLA membranes, which reduced the expression of inducible nitric-oxide synthase (iNOS) and matrix metalloproteinase-13 (MMP-13) in chondrocytes through

the synergistic effect of hydrostatic pressure and dexamethasone, however, *in vivo* effectiveness of the nanofibers was not explored. Similarly, Liang et al. [48] investigated the therapeutic potential of anti-oxidative PCL-grafted lignin (PCL-*g*-lignin)-based nanofibrous membranes for the treatment of OA. However, an open surgical procedure was performed in a rabbit OA model, which may hamper the utilization of electrospun scaffolds for minimally invasive treatment. Recently electrospinning combined with the electrospray technology has garnered significant attention of the research community to fabricate injectable nanofiber microspheres, which not only exhibits the versatility of electrospinning, but also broadens the variability of this technology [45]. The nanofiber microspheres fabricated in this study feature good geometrical compatibility and mechanical stability, which can be injected into the joint through minimally invasive approach, thus further extending the therapeutic potential of electrospun scaffolds for the treatment of OA.

Besides their good injectable effect, the drug-carrying properties of nanofiber microspheres are also desirable for the treatment of OA. To reveal whether MPNs affect the release behavior of TA from nanofiber microspheres, drug release assays were performed on TMS and TSMS in PBS *in vitro* (Fig. 3). The release rate of TA was found to be faster in TMS than that of the TSMS, which indicated that the MPNs conferred the sustained release characteristics to the microspheres, which may also have implications for the
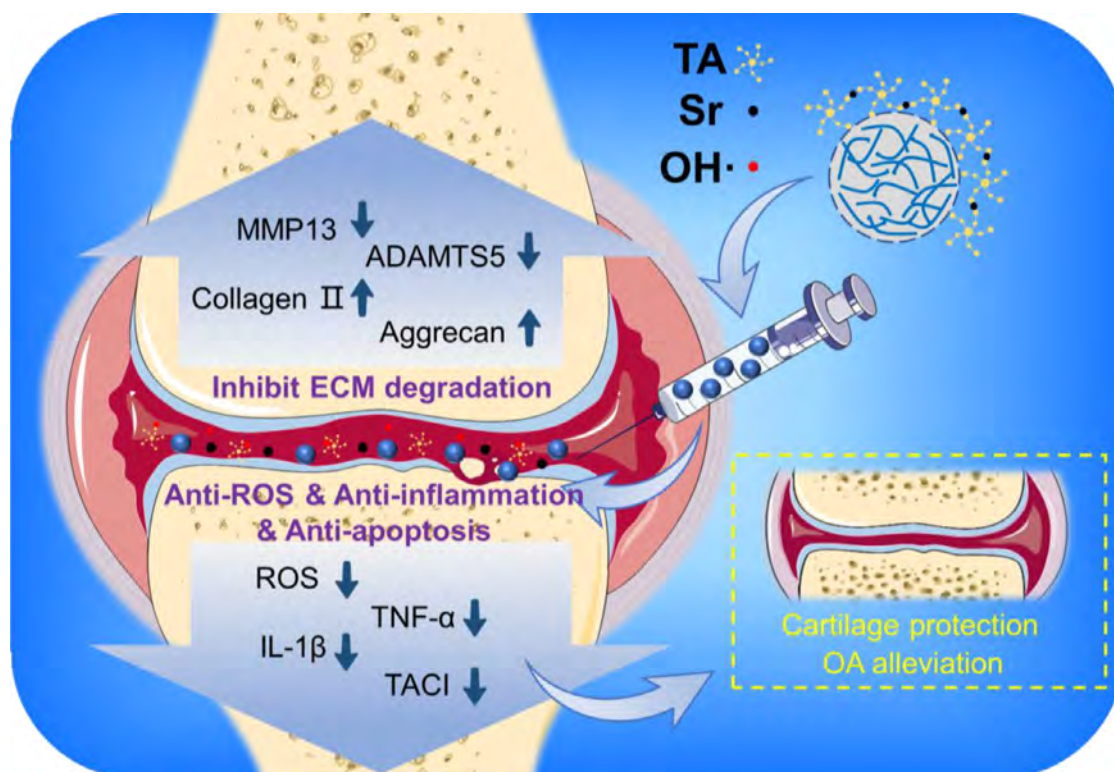
Fig. 9. Schematic illustration showing the roles of MPNs-modified nanofiber microspheres in alleviating osteoarthritis.

OA therapy. It has been reported that MPNs feature triggered drug release characteristics [49]. Metal ion cross-linking contributed to the retention of TA in the microspheres, while ionic interactions were disrupted, where the TA was protonated and released from the microspheres [50]. In striking contrast, the TMS, which lacked MPNs were devoid of ion-ion interaction, and therefore displayed an initial burst release of TA. An *in vitro* ROS scavenging assay further confirmed the sustained release characteristics of TSMS. The concentration of the released TA was increased with an increase in the incubation time of the TSMS; the extract solution obtained from the TSMS exhibited a higher ROS scavenging activity at 48 h than that of the 24 h.

The cytocompatibility of microspheres is the fundamental requirement for biomedical applications. Co-culture of chondrocytes along with the conditioned medium obtained from the microspheres showed negligible cytotoxicity and higher cell viability (> 80%) of all types of microspheres in the initial phase (Fig. 4). While insignificantly different, viability of the chondrocytes was lower in TMS and TSMS groups as compared to the control group. At day 3, the numbers of proliferating cells in the TA-modified groups were significantly lower than that of the control group. It has been previously reported that the high concentrations of TA (4 mg/mL) would cause cytotoxicity [51], which is detrimental to the cell proliferation. On the other hand, we employed relatively low concentration of TA to modify the microspheres (i.e., 3 mg/mL); the released amount of TA was considerably less (microgram per milliliter level), which did not adversely affect the viability of chondrocytes. However, in addition to scavenging free radicals, some catechins also act as inhibitors of the key enzymes in the cell cycle [52,53], which in turn may temporarily suppress the cell metabolism. Yang et al. [54] reported polyphenol epigallocatechin gallate (EGCG)-mediated inhibition of cell growth, which was ascribed to the non-specific binding of the EGCG to the cellular macromolecules. Nonetheless, these side effects of TA on the cell proliferation may not compromise the anti-oxidative ability of TA-

modified microspheres (Fig. 5 & 6). The H_2O_2 spontaneously forms highly reactive hydroxyl radicals, which attack DNA and lead to cytotoxicity or the production of the apoptotic DNA fragments [55]. Polyphenols have also been reported to eliminate H_2O_2-related reactive oxygen species (ROS) as well as downregulate the pro-apoptotic gene "caspase-3" and upregulate the expression of anti-apoptotic gene "BCL-2" [56,57]. Since phenols can react with the free radical species to delocalize unpaired electrons within the aromatic ring, The TA may plausibly scavenge the hydroxyl radicals through a resonance stabilization, thereby stimulating anti-apoptotic and antioxidant cell signaling pathways [58]. Therefore, the microspheres modified with TA exhibited inhibitory properties against inflammation-related genes as well as reduced the apoptosis of chondrocytes, which also have implications for the treatment of OA.

The pathogenesis for the development of OA is associated with multiple factors, including oxidative stress and inflammatory factors, which disrupt the synthesis of the cartilage matrix plausibly due to the inhibitory effect of the degradation-related enzymes [49]. Thus, the dual functions of anti-inflammation as well as the restoration of the cartilage synthesis and catabolic homeostasis are the mediators for the treatment of OA. The TA, as a plant derived polyphenol, has been widely exploited as an anti-inflammatory molecule, thanks to its good anti-inflammatory properties. The molecular mechanism by which TA retards the development of OA however yet remain to be explored. The TA acts as an antioxidant to inhibit the formation of hydroxyl radicals [59], and the high level of galloyl groups of the TA may inhibit the activity of degenerative enzymes (e.g. MMPs) [60]. In addition, polyphenols have the ability to quench lipid peroxidation and prevent oxidative DNA damage [61]. Therefore, TA-modified microspheres reduce the apoptosis of articular chondrocytes *in vivo*, plausibly via the phenol-mediated aromatic ring resonance stabilization to moderate free radical-induced damage (Fig. 8). Many metal salts play crucial role in the regeneration of tissues [62,63].

In OA, the balance between ECM synthesis and degradation is disturbed, which leads to tissue degeneration. Especially, an imbalance of the stromelysin and proteoglycans (PGs) has been shown to be the main pathological manifestation, with OA cartilage having higher levels of stromelysin while lower content of PG [64]. When the concentration of ions decreases below the physiological level, the rate of PG synthesis decreases. Consequently, the timely supplementation of cations has been shown to exert a promotional effect on chondrocytes in OA. Strontium ions, which are economical and stable as compared to growth factors and peptides, have been shown to stimulate the anabolism of human chondrocytes as well as promote cellular ECM secretion and inhibit OA development [65]. Therefore, TSMS-mediated higher cellular ECM production may be ascribed to the release of Sr^{2+} ions, which further translated into the best repair outcome in a rabbit OA model (Fig. 7).

The massive activation of osteoclasts might be closely correlated with joint inflammation and bone destruction [66]. The function of osteoclasts is mainly controlled by the balance between ligands, such as OPG/osteoclastogenesis inhibitory factor, RANKL, receptor activator of nuclear factor κB (RANK), and TNF-related apoptosis-inducing ligand (TRAIL) [67]. The RANKL is derived from synovial tissue and is mainly expressed on the surface of osteoblasts bound to RANK, which can promote osteoclastogenesis, osteoclast maturation and activation [68]. The OPG, produced by the osteoblasts, may regulate osteoclastogenesis and prevent RANKL-RANK interactions, thereby blocking the signaling pathways that lead to osteoclast differentiation and activation [69]. Our results showed that the animals treated with the TSMS exhibited higher concentration of OPG as compared to their counterparts treated with PBS, MS and TMS. On the other hand, the TA-modified microspheres significantly reduced RANKL levels along with the higher OPG/RANKL ratios compared to the PBS and MS groups, indicating that TA-modified microspheres may reduce osteoclast activation by releasing TA, while TSMS may also release strontium ions to enhance the expression of the OPG, further neutralizing the effects of osteoclasts.

5. Conclusion

In summary, we designed novel porous injectable nanofiber microspheres modified with TA or TA/Sr^{2+} MPNs via electrospraying for OA therapy. Modified microspheres demonstrated nanotopographical cues, stable structure, anti-oxidative properties and good cytocompatibility. Both the TMS and TSMS exhibited stronger free radicals scavenging ability and higher cell viability as well as less cell apoptosis in H_2O_2-induced inflammatory environment than that of the MS. More importantly, TSMS displayed good biological outcomes in comparison to the other groups as evidenced by the inhibition of cartilage degradation and promotion of cartilage-specific ECM secretion. Besides, TSMS displayed less expression of pro-inflammatory factors and cell apoptosis *in vitro* and *in vivo*. Taken together, this strategy of designing injectable microspheres and improving their biological performance based on electrospraying and MPNs modification may exert a therapeutic option for OA.

However, there are still several limitations in this study. Since the homogenized short nanofibers could not achieve a uniform length distribution, some short fibers with longer length may cause unstable electrospray, which may even clog the needles. Second, *in vivo* evaluation by using only rabbit model may not accurately replicate the anatomical structure of large animals. Therefore, evaluations of these microspheres in other animal models are warranted for their clinical translation. Finally, the exploitation of short nanofibers in the preparation of heterogeneous microspheres (e.g., multi-cavity microspheres, core-shell microspheres) requires more research to broaden the applications of microspheres in the biomedical field.

Declaration of Competing Interest

The authors declare that they have no known competing financial interests or personal relationships that could have appeared to influence the work reported in this paper.

Supplementary materials

Supplementary material associated with this article can be found, in the online version, at doi:10.1016/j.actbio.2022.11.040.

References

[1] W.H. Robinson, C.M. Lepus, Q. Wang, H. Raghu, R. Mao, T.M. Lindstrom, J. Sokolove, Low-grade inflammation as a key mediator of the pathogenesis of osteoarthritis, Nat. Rev. Rheumatol. 12 (2016) 580–592, doi:10.1038/nrrheum.2016.136.

[2] Y. Shi, X. Hu, J. Cheng, X. Zhang, F. Zhao, W. Shi, B. Ren, H. Yu, P. Yang, Z. Li, Q. Liu, Z. Liu, X. Duan, X. Fu, J. Zhang, J. Wang, Y. Ao, A small molecule promotes cartilage extracellular matrix generation and inhibits osteoarthritis development, Nat. Commun. (2019) 10, doi:10.1038/s41467-019-09839-x.

[3] Y.M. Lee, E. Son, S.H. Kim, O.S. Kim, D.S. Kim, Anti-inflammatory and antiosteoarthritis effect of Mollugo pentaphylla extract, Pharm. Biol. 57 (2019) 74–81, doi:10.1080/13880209.2018.1557700.

[4] D.J. Hunter, Pharmacologic therapy for osteoarthritis-the era of disease modification, Nat. Rev. Rheumatol. 7 (2011) 13–22, doi:10.1038/nrrheum.2010.178.

[5] Z. Zhang, T.W. Eyster, P.X. Ma, Nanostructured injectable cell microcarriers for tissue regeneration, Nanomedicine 11 (2016) 1611–1628, doi:10.2217/nnm-2016-0083.

[6] J.V. John, M. Choksi, S. Chen, S.K. Boda, Y. Su, A. McCarthy, M.J. Teusink, R.A. Reinhardt, J. Xie, Tethering peptides onto biomimetic and injectable nanofiber microspheres to direct cellular response, Nanomed. Nanotechnol., Biol. Med. 22 (2019) 102081, doi:10.1016/j.nano.2019.102081.

[7] X. Liu, X. Jin, P.X. Ma, Nanofibrous hollow microspheres self-assembled from star-shaped polymers as injectable cell carriers for knee repair, Nat. Mater. 10 (2011) 398–406, doi:10.1038/nmat2999.

[8] Y. Zhou, H.L. Gao, L.L. Shen, Z. Pan, L.B. Mao, T. Wu, J.C. He, D.H. Zou, Z.Y. Zhang, S.H. Yu, Chitosan microspheres with an extracellular matrix-mimicking nanofibrous structure as cell-carrier building blocks for bottom-up cartilage tissue engineering, Nanoscale 8 (2016) 309–317, doi:10.1039/c5nr06876b.

[9] J.V. John, A. McCarthy, H. Wang, S. Chen, Y. Su, E. Davis, X. Li, J.S. Park, R.A. Reinhardt, J. Xie, Engineering biomimetic nanofiber microspheres with tailored size, predesigned structure, and desired composition via gas bubble–mediated coaxial electrospray, Small 1907393 (2020), doi:10.1002/smll.201907393.

[10] M. Deng, S.G. Kumbar, L.S. Nair, A.L. Weikel, H.R. Allcock, C.T. Laurencin, Biomimetic structures: biological implications of dipeptide-substituted polyphosphazene-polyester blend nanofiber matrices for load-bearing bone regeneration, Adv. Funct. Mater. 21 (2011) 2641–2651, doi:10.1002/adfm.201100275.

[11] S.K. Boda, S. Chen, K. Chu, H.J. Kim, J. Xie, Electrospraying electrospun nanofiber segments into injectable microspheres for potential cell delivery, ACS Appl. Mater. Interfaces 10 (2018) 25069–25079, doi:10.1021/acsami.8b06386.

[12] J. Zhang, Y. Wang, Q. Qu, T. Lu, F. Li, J. Wang, A. Yang, Y. Zou, C. Huang, Preparation of single, heteromorphic microspheres, and their progress for medical applications, Macromol. Mater. Eng. 306 (2021) 1–17, doi:10.1002/mame.202000593.

[13] V. Kostyuk, A. Potapovich, C. De Luca, The promise of plant polyphenols as the golden standard skin anti-inflammatory agents, Curr. Drug Metab. 11 (2010) 415–424, doi:10.2174/138920010791526033.

[14] M. Shin, J.H. Ryu, J.P. Park, K. Kim, J.W. Yang, H. Lee, DNA/tannic acid hybrid gel exhibiting biodegradability, extensibility, tissue adhesiveness, and hemostatic ability, Adv. Funct. Mater. 25 (2015) 1270–1278, doi:10.1002/adfm.201403992.

[15] V. Kozlovskaya, E. Kharlampieva, I. Drachuk, D. Cheng, V.V. Tsukruk, Responsive microcapsule reactors based on hydrogen-bonded tannic acid layer-by-layer assemblies, Soft Matter 6 (2010) 3596–3608, doi:10.1039/b927369g.

[16] H. Ejima, J.J. Richardson, F. Caruso, Metal-phenolic networks as a versatile platform to engineer nanomaterials and biointerfaces, Nano Today 12 (2017) 136–148, doi:10.1016/j.nantod.2016.12.012.

[17] A. Larrañaga, I.L.M. Isa, V. Patil, S. Thamboo, M. Lomora, M.A. Fernández-Yague, J.R. Sarasua, C.G. Palivan, A. Pandit, Antioxidant functionalized polymer capsules to prevent oxidative stress, Acta Biomater. 67 (2018) 21–31, doi:10.1016/j.actbio.2017.12.014.

[18] V. Natarajan, B. Madhan, M.L. Tiku, Intra-articular injections of polyphenols protect articular cartilage from inflammation-induced degradation: suggesting a potential role in cartilage therapeutics, PLoS One 10 (2015), doi:10.1371/journal.pone.0127165.

[19] S.J. Michał Stuss, Ewa Sewerynek, Iwona Król, Wioletta Stępień-Kłos, Assessment of OPG, RANKL, bone turnover markers serum levels, and BMD after treatment with strontium ranelate and ibandronate in patients with postmenopausal osteoporosis, Endokrynol. Pol. 67 (2016) 174–184, doi:10.5603/EP.

[20] C. Wang, B. Chen, W. Wang, X. Zhang, T. Hu, Y. He, K. Lin, X. Liu, Strontium released bi-lineage scaffolds with immunomodulatory properties induce a pro-regenerative environment for osteochondral regeneration, Mater. Sci. Eng. C (2019) 103, doi:10.1016/j.msec.2019.109833.

[21] F. Zhao, B. Lei, X. Li, Y. Mo, R. Wang, D. Chen, X. Chen, Promoting in vivo early angiogenesis with sub-micrometer strontium-contained bioactive microspheres through modulating macrophage phenotypes, Biomaterials 178 (2018) 36–47, doi:10.1016/j.biomaterials.2018.06.004.

[22] J. Xie, C.H. Wang, Electrospray in the dripping mode for cell microencapsulation, J. Colloid Interface Sci. 312 (2007) 247–255, doi:10.1016/j.jcis.2007.04.023.

[23] Y. Zou, P. Wang, A. Zhang, Z. Qin, Y. Li, Y. Xianyu, H. Zhang, Covalent organic framework-incorporated nanofibrous membrane as an intelligent platform for wound dressing, ACS Appl. Mater. Interfaces 14 (2022) 8680–8692, doi:10.1021/acsami.1c19754.

[24] C. Guo, C. Li, D.L. Kaplan, Enzymatic degradation of Bombyx mori silk materials: a review, Biomacromolecules 21 (2020) 1678–1686, doi:10.1021/acs.biomac.0c00090.

[25] Y. Xu, D. Li, Z. Yin, A. He, M. Lin, G. Jiang, X. Song, X. Hu, Y. Liu, J. Wang, X. Wang, L. Duan, G. Zhou, Tissue-engineered trachea regeneration using decellularized trachea matrix treated with laser micropore technique, Acta Biomater. 58 (2017) 113–121, doi:10.1016/j.actbio.2017.05.010.

[26] G. Zhou, H. Jiang, Z. Yin, Y. Liu, Q. Zhang, C. Zhang, B. Pan, J. Zhou, X. Zhou, H. Sun, D. Li, A. He, Z. Zhang, W. Zhang, W. Liu, Y. Cao, In vitro regeneration of patient-specific ear-shaped cartilage and its first clinical application for auricular reconstruction, EBioMedicine 28 (2018) 287–302, doi:10.1016/j.ebiom.2018.01.011.

[27] P.X. Ling, L.N. Zhang, Y. Jin, Y.L. He, T.M. Zhang, Effects of a hyaluronic acid and low molecular weight heparin injection on osteoarthritis in rabbits, Drug Discov. Ther. 3 (2009) 146–150.

[28] A.M. McCoy, Animal models of osteoarthritis: comparisons and key considerations, Vet. Pathol. 52 (2015) 803–818, doi:10.1177/0300985815588611.

[29] K.P.H. Pritzker, S. Gay, S.A. Jimenez, K. Ostergaard, J.P. Pelletier, K. Revell, D. Salter, W.B. van den Berg, Osteoarthritis cartilage histopathology: grading and staging, Osteoarthr. Cartil. 14 (2006) 13–29, doi:10.1016/j.joca.2005.07.014.

[30] S.J. Moon, Y.J. Woo, J.H. Jeong, M.K. Park, H.J. Oh, J.S. Park, E.K. Kim, M.L. Cho, S.H. Park, H.Y. Kim, J.K. Min, Rebamipide attenuates pain severity and cartilage degeneration in a rat model of osteoarthritis by downregulating oxidative damage and catabolic activity in chondrocytes, Osteoarthr. Cartil. 20 (2012) 1426–1438, doi:10.1016/j.joca.2012.08.002.

[31] S. Lee, Y.Y. Chang, J. Lee, S.K. Madhurakkat Perikamana, E.M. Kim, Y.H. Jung, J.H. Yun, H. Shin, Surface engineering of titanium alloy using metal-polyphenol network coating with magnesium ions for improved osseointegration, Biomater. Sci. 8 (2020) 3404–3417, doi:10.1039/d0bm00566e.

[32] N. Ninan, A. Forget, V.P. Shastri, N.H. Voelcker, A. Blencowe, Antibacterial and anti-inflammatory pH-responsive tannic acid-carboxylated agarose composite hydrogels for wound healing, ACS Appl. Mater. Interfaces 8 (2016) 28511–28521, doi:10.1021/acsami.6b10491.

[33] S. Rashedi, S. Afshar, A. Rostami, M. Ghazalian, H. Nazockdast, Co-electrospun poly(lactic acid)/gelatin nanofibrous scaffold prepared by a new solvent system: morphological, mechanical and in vitro degradability properties, Int. J. Polym. Mater. Polym. Biomater. 70 (2021) 545–553, doi:10.1080/00914037.2020.1740987.

[34] M.O. Ilori, S.A. Adebusoye, O.O. Amund, B.O. Oyetoran, A study of tannic acid degradation by soil bacteria, Pakistan J. Biol. Sci. 10 (2007) 3224–3227, doi:10.3923/pjbs.2007.3224.3227.

[35] M. Li, X. Zi, Q. Diao, H. Hu, J. Tang, H. Zhou, Effect of tannic acids on the fermentation quality and aerobic stability of cassava foliage, Pratacultural Sci. 36 (2019) 1662–1667, doi:10.11829/j.issn.1001-0629.2018-0464.

[36] W. Chen, J. Ma, L. Zhu, Y. Morsi, H. Ei-hamshary, S.S. Al-deyab, X. Mo, Superelastic, superabsorbent and 3D nanofiber-assembled scaffold for tissue engineering, Colloids Surf. B Biointerfaces 142 (2016) 165–172, doi:10.1016/j.colsurfb.2016.02.050.

[37] S. Alippilakkotte, L. Sreejith, Benign route for the modification and characterization of poly(lactic acid) (PLA) scaffolds for medicinal application, J. Appl. Polym. Sci. 135 (2018) 1–13, doi:10.1002/app.46056.

[38] M. Xing, Y. Jiang, W. Bi, L. Gao, Y.L. Zhou, S.Le Rao, L.L. Ma, Z.W. Zhang, H.T. Yang, J. Chang, Strontium ions protect hearts against myocardial ischemia/reperfusion injury, Sci. Adv. 7 (2021) 1–19, doi:10.1126/sciadv.abe0726.

[39] H. Rodríguez, B. de las Rivas, C. Gómez-Cordovés, R. Muñoz, Degradation of tannic acid by cell-free extracts of Lactobacillus plantarum, Food Chem. 107 (2008) 664–670, doi:10.1016/j.foodchem.2007.08.063.

[40] P. Verma, K. Dalal, ADAMTS-4 and ADAMTS-5: key enzymes in osteoarthritis, J. Cell. Biochem. 112 (2011) 3507–3514, doi:10.1002/jcb.23298.

[41] M. Kapoor, J. Martel-Pelletier, D. Lajeunesse, J.P. Pelletier, H. Fahmi, Role of proinflammatory cytokines in the pathophysiology of osteoarthritis, Nat. Rev. Rheumatol. 7 (2011) 33–42, doi:10.1038/nrrheum.2010.196.

[42] T. Huang, S.H. Lin, N.M. Malewicz, Y. Zhang, Y. Zhang, M. Goulding, R.H. LaMotte, Q. Ma, Identifying the pathways required for coping behaviours associated with sustained pain, Nature 565 (2019) 86–90, doi:10.1038/s41586-018-0793-8.

[43] Y. Chen, M. Sha, M. Liu, Y. Morsi, X. Mo, Advanced fabrication for electrospun three-dimensional nanofiber aerogels and scaffolds, Bioact. Mater. 5 (2020) 963–979, doi:10.1016/j.bioactmat.2020.06.023.

[44] Y. Chen, W. Xu, M. Shafiq, D. Song, X. Xie, Z. Yuan, M. EL-Newehy, H. EL-Hamshary, Y. Morsi, Y. Liu, X. Mo, Chondroitin sulfate cross-linked three-dimensional tailored electrospun scaffolds for cartilage regeneration, Mater. Sci. Eng. C (2022) 112643, doi:10.1016/j.msec.2022.112643.

[45] Y. Chen, X. Dong, M. Shafiq, G. Myles, N. Radacsi, X. Mo, Recent advancements on three – dimensional electrospun nanofiber scaffolds for tissue engineering, Adv. Fiber Mater. (2022), doi:10.1007/s42765-022-00170-7.

[46] Y. Lei, Y. Wang, J. Shen, Z. Cai, C. Zhao, H. Chen, X. Luo, N. Hu, W. Cui, W. Huang, Injectable hydrogel microspheres with self-renewable hydration layers alleviate osteoarthritis, Sci. Adv. 8 (2022), doi:10.1126/sciadv.abl6449.

[47] S. Ansari, A. Karkhaneh, S. Bonakdar, N. Haghighipour, Simultaneous effects of hydrostatic pressure and dexamethasone release from electrospun fibers on inflammation-induced chondrocytes, Eur. Polym. J. 118 (2019) 244–253, doi:10.1016/j.eurpolymj.2019.06.003.

[48] R. Liang, J. Zhao, B. Li, P. Cai, X.J. Loh, C. Xu, P. Chen, D. Kai, L. Zheng, Implantable and degradable antioxidant poly(ε-caprolactone)-lignin nanofiber membrane for effective osteoarthritis treatment, Biomaterials 230 (2020) 119601, doi:10.1016/j.biomaterials.2019.119601.

[49] Ş. Sungur, A. Uzar, Investigation of complexes tannic acid and myricetin with Fe(III), Spectrochim. Acta - Part A Mol. Biomol. Spectrosc. 69 (2008) 225–229, doi:10.1016/j.saa.2007.03.038.

[50] H. Liang, Y. Pei, J. Li, W. Xiong, Y. He, S. Liu, Y. Li, B. Li, pH-Degradable antioxidant nanoparticles based on hydrogen-bonded tannic acid assembly, RSC Adv. 6 (2016) 31374–31385, doi:10.1039/c6ra02527g.

[51] Y. Li, M. Chen, J. Yan, W. Zhou, S. Gao, S. Liu, Q. Li, Y. Zheng, Y. Cheng, Q. Guo, Tannic acid/Sr2+-coated silk/graphene oxide-based meniscus scaffold with anti-inflammatory and anti-ROS functions for cartilage protection and delaying osteoarthritis, Acta Biomater. 126 (2021) 119–131, doi:10.1016/j.actbio.2021.02.046.

[52] D. Li, Z. Liu, Y. Yuan, Y. Liu, F. Niu, Green synthesis of gallic acid-coated silver nanoparticles with high antimicrobial activity and low cytotoxicity to normal cells, Process Biochem. 50 (2015) 357–366, doi:10.1016/j.procbio.2015.01.002.

[53] V. Ugartondo, M. Mitjans, C. Lozano, J.L. Torres, M.P. Vinardell, Comparative study of the cytotoxicity induced by antioxidant epicatechin conjugates obtained from grape, J. Agric. Food Chem. 54 (2006) 6945–6950, doi:10.1021/jf061356i.

[54] C.S. Yang, S. Sang, J.D. Lambert, M.J. Lee, Bioavailability issues in studying the health effects of plant polyphenolic compounds, Mol. Nutr. Food Res. 52 (2008) 139–151, doi:10.1002/mnfr.200700234.

[55] C.V. Suschek, O. Schnorr, K. Hemmrich, O.A. Lars-Oliver Klotz, H. Sies, V. Kolb-Bachofen, Critical role of L-arginine in endothelial cell survival during oxidative stress, Circulation 107 (2003) 2607–2614, doi:10.1161/01.cir.0000066909.13953.f1.

[56] X. Yan, Y. Li, H. Yu, W. Wang, C. Wu, Y. Yang, Y. Hu, X. Shi, J. Li, Epigallocatechin-3-gallate inhibits H2O2-induced apoptosis in Mouse Vascular Smooth Muscle Cells via 67kD Laminin Receptor, Sci. Rep. 7 (2017) 1–10, doi:10.1038/s41598-017-08301-6.

[57] S. Lee, J. Lee, H. Byun, S. jeong Kim, J. Joo, H.H. Park, H. shin, Evaluation of the anti-oxidative and ROS scavenging properties of biomaterials coated with epigallocatechin gallate for tissue engineering, Acta Biomater. 124 (2021) 166–178, doi:10.1016/j.actbio.2021.02.005.

[58] I.P. Shanura Fernando, M. Kim, K.T. Son, Y. Jeong, Y.J. Jeon, Antioxidant activity of marine algal polyphenolic compounds: a mechanistic approach, J. Med. Food 19 (2016) 615–628, doi:10.1089/jmf.2016.3706.

[59] R.G. Andrade, L.T. Dalvi, J.M.C. Silva, G.K.B. Lopes, A. Alonso, M. Hermes-Lima, The antioxidant effect of tannic acid on the in vitro copper-mediated formation of free radicals, Arch. Biochem. Biophys. 437 (2005) 1–9, doi:10.1016/j.abb.2005.02.016.

[60] R.R. Liu, M. Fang, L. Zhang, C.F. Tang, Q. Dou, J.H. Chen, Anti-proteolytic capacity and bonding durability of proanthocyanidin-biomodified demineralized dentin matrix, Int. J. Oral Sci. 6 (2014) 168–174, doi:10.1038/ijos.2014.22.

[61] M. Lodovici, F. Guglielmi, C. Casalini, M. Meoni, V. Cheynier, P. Dolara, Antioxidant and radical scavenging properties in vitro of polyphenolic extracts from red wine, Eur. J. Nutr. 40 (2001) 74–77, doi:10.1007/PL00007386.

[62] K. Glenske, P. Donkiewicz, A. Köwitsch, N. Milosevic-Oljaca, P. Rider, S. Rofall, J. Franke, O. Jung, R. Smeets, R. Schnettler, S. Wenisch, M. Barbeck, Applications of metals for bone regeneration, 2018. doi:10.3390/ijms19030826.

[63] R. Yang, Y. Zheng, Y. Zhang, G. Li, Y. Xu, Y. Zhang, Y. Xu, C. Zhuang, P. Yu, L. Deng, W. Cui, Y. Chen, L. Wang, Bipolar metal flexible electrospun fibrous membrane based on metal–organic framework for gradient healing of tendon-to-bone interface regeneration, Adv. Healthc. Mater. 11 (2022) 1–14, doi:10.1002/adhm.202200072.

[64] Y. Henrotin, A. Labasse, S.X. Zheng, P. Galais, Y. Tsouderos, J.M. Crielaard, J.Y. Reginster, Strontium ranelate increases cartilage matrix formation, J. Bone Miner. Res. 16 (2001) 299–308, doi:10.1359/jbmr.2001.16.2.299.

[65] Y. Li, M. Chen, W. Zhou, S. Gao, X. Luo, L. Peng, J. Yan, P. Wang, Q. Li, Y. Zheng, S. Liu, Y. Cheng, Q. Guo, Cell-free 3D wet-electrospun PCL/silk fibroin/Sr2+ scaffold promotes successful total meniscus regeneration in a rabbit model, Acta Biomater. (2020), doi:10.1016/j.actbio.2020.06.017.

[66] Y. Abu-Amer, S. Abbas, T. Hirayama, TNF receptor type 1 regulates RANK ligand expression by stromal cells and modulates osteoclastogenesis, J. Cell. Biochem. 93 (2004) 980–989, doi:10.1002/jcb.20197.

[67] L.C. Hofbauer, A.E. Heufelder, The role of osteoprotegerin and receptor activator of nuclear factor κB ligand in the pathogenesis and treatment of rheumatoid arthritis, Arthritis Rheum. 44 (2001) 253–259, doi:10.1002/1529-0131(200102)44:2<253::AID-ANR41>3.0.CO;2-S.

[68] N. Saidenberg-Kermanac'H, A. Corrado, D. Lemeiter, M.C. Devernejoul, M.C. Boissier, M.E. Cohen-Solal, TNF-α antibodies and osteoprotegerin decrease systemic bone loss associated with inflammation through distinct mechanisms in collagen-induced arthritis, Bone 35 (2004) 1200–1207, doi:10.1016/j.bone.2004.07.004.

[69] A. Corrado, N. Maruotti, F.P. Cantatore, Osteoblast role in rheumatic diseases, Int. J. Mol. Sci. (2017) 18, doi:10.3390/ijms18061272.